

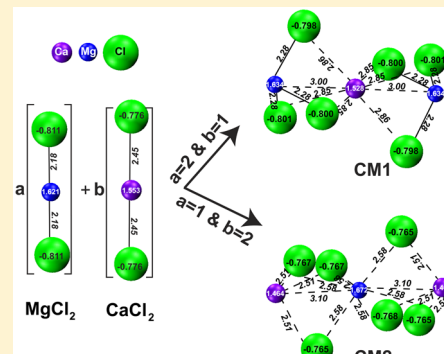
# First-Principles Study of Chemical Mixtures of $\text{CaCl}_2$ and $\text{MgCl}_2$ Hydrates for Optimized Seasonal Heat Storage

A. D. Pathak,<sup>ID</sup> I. Tranca, S. V. Nedea,<sup>\*</sup> H. A. Zondag, C. C. M. Rindt, and D. M. J. Smeulders

Energy Technology, Department of Mechanical Engineering, Eindhoven University of Technology, Eindhoven 5612 AZ, The Netherlands

 Supporting Information

**ABSTRACT:** Chloride-based salt hydrates form a promising class of thermochemical materials (TCMs), having high storage capacity and fast kinetics. In the charging cycles of these hydrates however hydrolysis might appear along with dehydration. The HCl produced during the hydrolysis degrades and corrodes the storage system. Our GGA-DFT results show that the enthalpy change during proton formation (an important step in hydrolysis) is much higher for  $\text{CaCl}_2 \cdot 2\text{H}_2\text{O}$  (33.75 kcal/mol) than for  $\text{MgCl}_2 \cdot 2\text{H}_2\text{O}$  (19.55 kcal/mol). This is a strong indicator that hydrolysis can be minimized by appropriate chemical mixing of  $\text{CaCl}_2$  and  $\text{MgCl}_2$  hydrates, which is also confirmed by recent experimental studies. GGA-DFT calculations were performed to obtain and analyze the optimized structures, charge distributions, bonding indicators and harmonic frequencies of various chemical mixtures hydrates and compared them to their elementary salts hydrates. We have further assessed the equilibrium products concentration of dehydration/hydrolysis of the chemical mixtures under a wide range of operating conditions. We observed that chemical mixing leads to an increase of the onset hydrolysis temperature with a maximum value of 79 K, thus increasing the resistance against hydrolysis with respect to the elementary salt hydrates. We also found that the chemical mixing of  $\text{CaCl}_2$  and  $\text{MgCl}_2$  hydrates widens the operating dehydration temperature range by a maximum value of 182 K ( $\text{CaMg}_2\text{Cl}_6 \cdot 2\text{H}_2\text{O}$ ) and lowers the binding enthalpy with respect to the physical mixture by  $\approx 65$  kcal/mol for TCM based heat storage systems.



## INTRODUCTION

The European Union has set as target that 20% of the final energy consumption should be supplied by renewable energy by 2020.<sup>1</sup> Solar energy is one of the cleanest renewable energy resources with the least negative impact on the environment. Solar energy can be stored in chemical form or in physical form. Thermal energy can be stored in its physical form as sensible heat and latent heat.<sup>2,3</sup> In chemical form, thermal energy can be stored using a reversible chemical reaction, known as thermochemical heat storage. The energy storage density of the thermochemical form is higher (up to 20 times) than that of the physical form.<sup>4,5</sup>

Salt– $\text{H}_2\text{O}$  (salt hydrates), oxide– $\text{H}_2\text{O}$ , oxide– $\text{CO}_2$ , salt– $\text{NH}_3$  and peroxide–oxide reaction pairs are widely explored options for thermochemical heat storage materials.<sup>3,6–11</sup> Unlike  $\text{CO}_2$  and  $\text{NH}_3$ , water is readily available and is a nontoxic working fluid. However, for water-based working fluids, dehydration reactions of hydroxides ( $\text{M}(\text{OH})_2$ ,  $\text{M} = \text{Ca/Mg}$ ) take place at higher temperatures ( $>600$  K).<sup>12,13</sup> Peroxide–oxide based redox reaction pair operates at an even higher temperature ( $>773$  K).<sup>10,11</sup> Thus, they are less suitable for providing thermal comfort in the built environment using solar energy. Salt hydrates, on the other hand, have lower equilibrium dehydration temperature in combination with high energy storage density and can be used for seasonal

solar heat storage. Chloride-based salt hydrates are one class of TCMs with high storage capacity and fast reaction kinetics.  $\text{MgCl}_2$  and  $\text{CaCl}_2$  hydrates are the two most promising reversible materials among chloride-based hydrates for seasonal heat storage.<sup>6</sup> However, these chloride-based salt hydrates suffer from irreversible hydrolysis as a side reaction. Hydrolysis produces corrosive HCl gas and affects the performance of the heat storage system.

In practical applications, hydrolysis can be potentially avoided by using a complex compound/double salt that will shift the process to a higher temperature. For example, industrially Mg is produced electrolytically from pure anhydrous  $\text{MgCl}_2$ . Hydrolysis is a major concern in the production of anhydrous  $\text{MgCl}_2$  from dehydration of  $\text{MgCl}_2 \cdot 6\text{H}_2\text{O}$ .<sup>14</sup> Dolezal<sup>15</sup> proposed a method to reduce hydrolysis by forming a complex compound ( $\text{MgCl}_2 \cdot \text{C}_6\text{H}_5\text{NH}_2 \cdot \text{HCl} \cdot 6\text{H}_2\text{O}$ ) with amine hydrochlorides. In the case of  $\text{MgCl}_2 \cdot 6\text{H}_2\text{O}$ , hydrolysis can be reduced by replacing  $\text{H}_2\text{O}$  with  $\text{NH}_3$ .<sup>16</sup> Alternatively, it can be shifted to a higher temperature by using a double salt like  $\text{MgCl}_2 \cdot \text{NH}_4\text{Cl} \cdot 6\text{H}_2\text{O}$ .<sup>17,18</sup>

Received: May 30, 2017

Revised: August 9, 2017

Published: August 28, 2017

Doping and mixing are two approaches to improve the durability of TCMs. Doping of halides in salt hydrates is used to improve their dehydration kinetics and retard hydrolysis.<sup>19</sup> Doping of various salts like chlorides, acetates, sulfates, and nitrates has been investigated in order to assess their effect on dehydration temperature of  $\text{Mg}(\text{OH})_2$  and  $\text{Ca}(\text{OH})_2$ . Among these dopants, nitrates are found to be effective in decreasing the dehydration temperature and accelerating the dehydration kinetics of hydroxides.<sup>20</sup> The selection of the dopant can be made either by using a scientific approach or by chemical intuition.<sup>21</sup> However, doping of salt hydrates has not been investigated to date in a systematic way.

Mixing of salt hydrates to improve their performance and stability is the other emerging approach.<sup>22–25</sup> A limitation of this approach can be the appearance of phase segregation, which can reduce the efficiency and the reversibility of the cycles. A mixture of  $\text{MgSO}_4$  and  $\text{MgCl}_2$  hydrates has experimentally been shown to improve the hydration rate and enhance the temperature lift when compared with their elementary components ( $\text{MgSO}_4$  and  $\text{MgCl}_2$  hydrates).<sup>24</sup> Rammelberg<sup>23</sup> et al. have also observed experimentally that a mixture of  $\text{CaCl}_2$  and  $\text{MgCl}_2$  hydrates shows improved kinetics and better stability than their elementary  $\text{MgCl}_2$  and  $\text{CaCl}_2$  hydrates.

A mixture of salt hydrates can occur either at grain level (physical mixture) or at a molecular level (chemical mixture) or as combination of both. If the mixture modifies the molecular structure of the salt, it is called chemical mixture/double salt.  $\text{CaCl}_2$  and  $\text{MgCl}_2$  salts can form two types of chemical mixtures<sup>26–28</sup> in the molar ratio of 1:2 (CM1,  $\text{CaCl}_2 \cdot 2\text{MgCl}_2$ ) and 2:1 (CM2,  $2\text{CaCl}_2 \cdot \text{MgCl}_2$ ) as shown in Figure 1. These

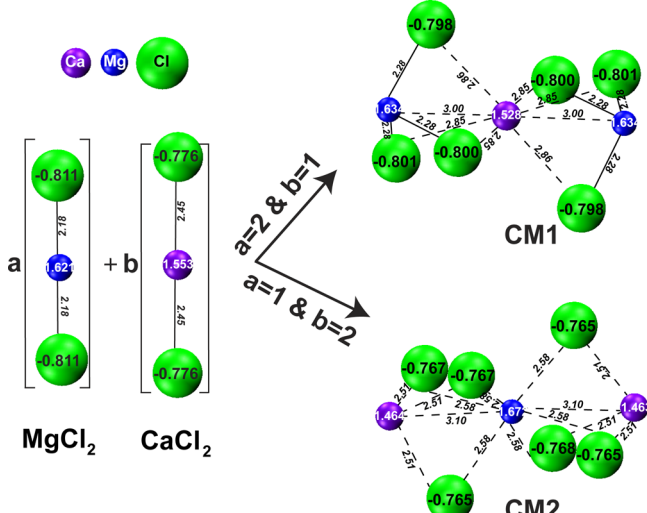
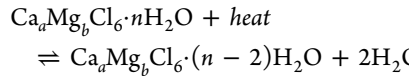


**Figure 1.** Optimized structures of the anhydrous elementary salts and chemical mixtures of  $\text{CaCl}_2$  and  $\text{MgCl}_2$ . Bond lengths  $<2.5 \text{ \AA}$  and  $>2.5 \text{ \AA}$  are represented as continuous and broken lines, respectively. The Bader atomic charges are also displayed.

chemical mixtures (CMs) could exist in various hydrates, with hydration number ( $n$ ) varying from 1 to 12. In the following text, the hydrates with  $n$  from 1 to 6 will be called lower hydrates while the ones with  $n$  from 8 to 12 will be called higher hydrates. The only experimentally investigated hydrate of these chemical mixtures is tachyhydrite ( $\text{CaMg}_2\text{Cl}_6 \cdot 12\text{H}_2\text{O}$ ). This is a hygroscopic material, naturally found in evaporite

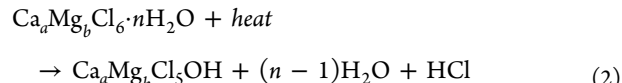
deposits and cretaceous potash formations.<sup>29,30</sup> The other hydrates of CM1 or CM2 are still to be experimentally explored.

The operating principle of the hydrated chemical mixture can be expressed as



$$[a, b = 1, 2; a + b = 3; n = 2, 4, 6, 8, 10, 12] \quad (1)$$

Hydrolysis, an irreversible competitive side reaction alongside with dehydration, can be expressed as



Computational models have been used to investigate the physical, dynamic and equilibrium properties of various salt hydrates from atomic to continuum level.<sup>31–36</sup> However, for the chemical mixtures a computational systematic investigation is presently still missing. A first-principles density functional theory (DFT) based study can be a good choice for a systematic molecular level understanding of the chemical salt hydrate mixtures.

In this study, we present the DFT optimized geometries of the chemical mixtures of  $\text{CaCl}_2$  and  $\text{MgCl}_2$ . The relative stability of their hydrates is assessed by DFT. We have systematically investigated the structural properties and atomic charges for all hydrates. Further, we have estimated their binding, dehydration and hydrolysis enthalpies. The bonding strengths of  $\text{Ca/Mg}-\text{Cl}$  and  $\text{Ca/Mg}-\text{O}$  pairs have been quantified by various bond indicators like bond order, electron density at the bond critical points, and crystal orbital Hamiltonian population analysis.<sup>37–48</sup> We have also obtained the harmonic frequencies of all the chemical mixture hydrates. On the basis of these values we estimated the Gibbs free energy ( $G$ ) of each molecule. Subsequently, we have obtained the equilibrium product concentration of dehydration and hydrolysis reactions under various conditions of temperature and pressure. The equilibrium curves of the chemical mixtures are compared with their elementary salt hydrates over a wide range of operating conditions. The onset temperatures for hydrolysis (HCl formation) of all hydrates of the salt mixtures are also obtained and compared with those of the elementary salt hydrates with similar hydration number.

## METHODOLOGY AND COMPUTATIONAL DETAILS

First-principles DFT calculations are performed using Perdew–Wang exchange and correlation functional (PW91),<sup>49</sup> as implemented in the Amsterdam density functional (ADF) program.<sup>50</sup> The exchange-correlation energy is calculated under the generalized gradient approximation (GGA) using a double-polarized triple- $\zeta$  basis set.<sup>51</sup> The GGA-DFT method at the PW91 or PBE level is known to reproduce accurately the structural, magnetic, thermal and thermodynamic properties of Mg and Ca based salt hydrates.<sup>31–33,35,52,53</sup>

In the present study, the molecular structures of the chemical mixtures  $\text{Ca}_a\text{Mg}_b\text{Cl}_6 \cdot n\text{H}_2\text{O}$  [ $a, b = 1, 2; a + b = 3; n = 0, 2, 4, 6, 8, 10, 12$ ] are fully optimized with GGA-DFT. The harmonic frequencies of the optimized geometries are obtained in order to estimate the vibrational, rotational, and translational contributions to the energy. The enthalpy change in the

reversible dehydration reactions (refer to eq 1) of the chemical mixtures per mole of H<sub>2</sub>O can be expressed as

$$E_{Dehyd} = 0.5 \times [E_{\text{Ca}_a\text{Mg}_b\text{Cl}_c \cdot (n-2)\text{H}_2\text{O}} + 2 \times E_{\text{H}_2\text{O}} - E_{\text{Ca}_a\text{Mg}_b\text{Cl}_c \cdot n\text{H}_2\text{O}}] \\ [a, b = 1, 2; a + b = 3; n = 2, 4, 6, 8, 10, 12] \quad (3)$$

The enthalpy change in the irreversible side reaction (hydrolysis, refer to eq 2) of the chemical mixture can be expressed as

$$E_{\text{Hydro}} = E_{\text{Ca}_a\text{Mg}_b\text{Cl}_c \cdot \text{OH}} + (n - 1) \times E_{\text{H}_2\text{O}} + E_{\text{HCl}} - E_{\text{Ca}_a\text{Mg}_b\text{Cl}_c \cdot n\text{H}_2\text{O}} \quad (4)$$

Similarly, the enthalpy change in binding of *n* water molecules to the anhydrous salt mixture can be obtained from

$$E_{\text{Bind}} = E_{\text{Ca}_a\text{Mg}_b\text{Cl}_c} + (n) \times E_{\text{H}_2\text{O}} - E_{\text{Ca}_a\text{Mg}_b\text{Cl}_c \cdot n\text{H}_2\text{O}} \quad (5)$$

Here *E* is the electronic ground state energy of an optimized molecule. The Gibbs free energy calculation is described in the *Supporting Information*. Δ*G* of the thermal decomposition can be expressed as

$$\Delta G = \sum G_{\text{prod}} - \sum G_{\text{reac}} \quad (6)$$

where *G<sub>prod</sub>* and *G<sub>reac</sub>* are the product and the reactant Gibbs free energy, respectively. The equilibrium concentration can be estimated by setting Δ*G* to zero. The state of matter (reactant/product) at given temperature (*T*) and pressure (*p*) is essential to estimate Δ*G* of a reaction. The products of thermolysis reactions (dehydration/hydrolysis) such as H<sub>2</sub>O and HCl exist in the gaseous phase in the operating conditions. CaMg<sub>2</sub>Cl<sub>6</sub> · 12H<sub>2</sub>O is the only double salt with a known crystal structure from experiments.<sup>29</sup> For the other hydrates of the chemical mixture, the crystal structures are still unexplored. The solid state crystal structure of a compound can be theoretically predicted from evolutionary algorithms in the light of similar known structures.<sup>54</sup> However, the CM1 and CM2 hydrates have five constituting atom types and may have a few hundred atoms in their unit cell. Under these conditions the computational prediction of the solid state crystal structure is quite challenging. However, the ideal gas phase assumption has been used to assess the equilibrium properties of the MgCl<sub>2</sub> and CaCl<sub>2</sub> hydrates, that were in agreement with the experiments.<sup>31,52</sup> Moreover, while the chemical mixture exists in solid phase for solar applications, it might exist in gas phase for metallurgical applications. Therefore, understanding the gas phase reactions can provide an important insight into the effect of chemical mixing.

For MgCl<sub>2</sub> hydrates, hydrolysis usually happens in the liquid phase of the salt hydrates mixture<sup>14</sup> and equilibrium concentrations of MgCl<sub>2</sub> hydrates from thermolysis were previously successfully investigated using the ideal gas phase assumption.<sup>31</sup> Since MgCl<sub>2</sub> is one of the elementary salt hydrates, the ideal gas assumption should hold true for the chemical mixture also. Thus, Δ*G* can be estimated by Gibbs free energy of the gaseous phase (*G<sub>gas</sub>*) of the reacting species. A first-principles equilibrium thermodynamic study of thermolysis of the chemical mixtures hydrates can qualitatively predict the effect of chemical mixing when compared to their elementary salt hydrates, found under the same simulation conditions. Furthermore, the results of this preliminary study

will determine the safety limits of these reactions in seasonal heat storage systems.

Besides the investigation of electronic and thermodynamic properties, a thorough analysis of the chemical bonding and interactions present in the studied systems has been performed. The bonding analysis has been performed by examining the bond order (BO), Bader atomic charges, electron density (ED), and Laplacian (*L*) values at the bond critical points (BCPs), as well as the crystal orbital Hamiltonian population (COHP) and crystal orbital overlap population (COOP) functions.<sup>37–48</sup> The Bader charges are a measure of the electron occupation on an atom, and therefore offer information on the charge transfer (e.g., on the ionic contributions to the chemical bond). The electron density values at the BCP probe the covalent energy contribution to the chemical bond. The Laplacian sign and values at the critical points offer further indications on the covalency/ionicity character of a bond. Thus, when the *L* value at the bond critical point is negative, the bond can be considered covalent, while when it is positive the bond has mainly a close-shell character (e.g., ionic bond, hydrogen bonding, van der Waals interactions).

Qualitative information on the bond characteristics can be additionally obtained from the COHP and COOP functions. The COHP function measures the sign and magnitude of the bond order energy overlap between atomic orbitals located on different atoms.<sup>46–48</sup> This enables the determination of the bonding, antibonding, or nonbonding character of the orbitals interaction, as well as the strength of the interaction:

$$-\text{COHP}_{ij}(E) = H_{ij} \sum_n c_i^n c_j^n \delta(E - E_n) \quad (7)$$

Here *H<sub>ij</sub>* is the Hamiltonian matrix element between atomic orbitals  $\phi_i$  and  $\phi_j$ . For positive values of  $-\text{COHP}_{ij}(E)$ , the electronic interactions between the two atomic orbitals are of bonding type. Negative values of  $-\text{COHP}_{ij}(E)$  describe an antibonding type of interaction, while a zero value is associated with the nonbonding interaction regime. The integrated value is equal to the contribution to the bond energy of the interaction of atomic orbitals *i* and *j*, apart from a correction due to differences in electrostatic interactions.<sup>55</sup>

The COOP function, defined by Hoffmann,<sup>56</sup> is related to  $-\text{COHP}_{ij}(E)$ :

$$\text{COOP}_{ij}(E) = S_{ij} \sum_n c_i^n c_j^n \delta(E - E_n) \quad (8)$$

$$S_{ij} = \langle \phi_i | \phi_j \rangle \quad (9)$$

where *S<sub>ij</sub>* is the overlap of atomic orbitals  $\phi_i$  and  $\phi_j$ . The values of  $\text{COOP}_{ij}(E)$  are also a measure of the bonding or antibonding character of an orbital fragment, but the bond order density is now weighted by the atomic orbital overlap *S<sub>ij</sub>* instead of the bond energy overlap *H<sub>ij</sub>*.

## RESULTS AND DISCUSSION

**Molecular Structures of Chemical Mixture.** The DFT/PW91 optimized geometries of CM1 and CM2 are shown in Figure 1. During the geometry optimization of these structures, no symmetry constraints have been imposed, and the vibrational frequencies have been computed to validate the found minima.

In the CM1 structure the Ca atom is situated in the center of the double salt, with the two Mg atoms positioned at equal distance (3.00 Å) with respect to the Ca atom. The Cl atoms

position closer to the Mg atoms (2.28 Å) than to the Ca atom (2.85 Å). Compared with the elementary salts, the interatomic distance between Mg and Cl is 4.6% larger in the CM1 than in the  $\text{MgCl}_2$  elementary salt, while the Ca–Cl interatomic distance is 16.3% larger in the CM1 than in the  $\text{CaCl}_2$  elementary salt. The average Bader charge on Cl in CM1 is similar to that of Cl in  $\text{MgCl}_2$ , while the average Bader charge on Mg and Ca is similar to that on their correspondent atoms from the elementary  $\text{MgCl}_2$  and  $\text{CaCl}_2$  salts (see Figure 1). The Coulombic interaction between Mg and Cl in CM1 is similar to the Mg–Cl pair in  $\text{MgCl}_2$ . The enthalpy of formation of CM1, if it forms from its elementary salts ( $\text{CaCl}_2$  and  $\text{MgCl}_2$ ), is −65.5 kcal/mol. This suggests that the formation of this chemical mixture is thermodynamically stable.

In the CM2 structure, the Mg atom is the one situated in the center of the double salt, with the two Ca atoms positioned at equal distance (3.10 Å) with respect to the Mg atom. The Cl atoms are situated slightly closer to the Ca atoms (2.51 Å) than to the Mg atom (2.58 Å). Compared with the elementary salts, the interatomic distance between Ca and Cl is 2.4% larger in the CM2 than in the  $\text{CaCl}_2$  elementary salt, while the Mg–Cl interatomic distance is 18.4% larger in the CM2 than in the  $\text{MgCl}_2$  elementary salt. The average Bader charge on Cl in CM2 is similar to that of Cl in  $\text{CaCl}_2$ , while the average Bader charge on Mg and Ca is, like for CM1, similar to their correspondent atoms from the elementary  $\text{MgCl}_2$  and  $\text{CaCl}_2$  salts (see Figure 1). The enthalpy of formation of CM2, if it forms from its elementary salts ( $\text{CaCl}_2$  and  $\text{MgCl}_2$ ), is −69.1 kcal/mol.

If  $\text{H}_2\text{O}$  molecules are successively hydrated to the outer Mg and Ca atoms of CM1 and CM2, each Mg/Ca atom present in the outer shell can accommodate up to 6  $\text{H}_2\text{O}$  molecules in the first hydration layer. Thus, for example, for CM1 which has 2 outer Mg atoms, 12 hydrated states are possible. The optimized structures (additionally, tables with all the bond lengths are provided in the Supporting Information) of the hydrated CM1 are shown in Figure 2 (for hydration number  $n = 2, 6, 12$ ) and in Figures S1 and S2 of the Supporting Information (for hydration number  $n = 1, 4, 8, 10$ ). Within these hydrated structures, the average interatomic distance between Mg and O in CM1 is observed to vary slightly from 2.05 to 2.11 Å as the hydration number  $n$  varies from 1 to 12 (see Figure 3a). This suggests that the Mg–O bond length is not significantly affected by the increase in  $n$  for CM1 hydrates. The only known experimental crystalline phase, that of  $\text{CM1}\cdot 12\text{H}_2\text{O}$ , has Mg–O coordination lengths of 2.01 and 2.10 Å. Thus, the found GGA-DFT optimized distances for the hydrate are in very good agreement with the experimental crystal data.<sup>29</sup> Compared with the elementary hydrates, we notice that the interatomic distance of the Mg–O pair in  $\text{MgCl}_2$  hydrates varies between 2.08 and 2.10 Å as  $n$  varies from 2 to 6 (see Figure 3a). Thus, the Mg–O bond length in the lower hydrates of CM1 is similar to that found in  $\text{MgCl}_2$  hydrates.

Depending on the hydration, the average Mg–Cl distance in CM1 varies from 2.28 to 3.86 Å as  $n$  varies from 0 to 12 (see Figure 3b). The average Mg–Cl interatomic distance increases more significantly (0.61 Å) by increasing  $n$  from 6 to 8. Higher hydration numbers in CM1 ( $n > 6$ ) push the Cl atoms further apart from the Mg atom. In  $\text{MgCl}_2$  hydrates, the average Mg–Cl interatomic distance varies similarly from 2.18 to 3.76 Å as  $n$  varies from 0 to 6 (see Figure 3b). The Mg–Cl distances in CM1 and in  $\text{MgCl}_2$  are observed to be similar up to the tetrahydrates. The Mg–Cl interatomic distance in hexahydrates

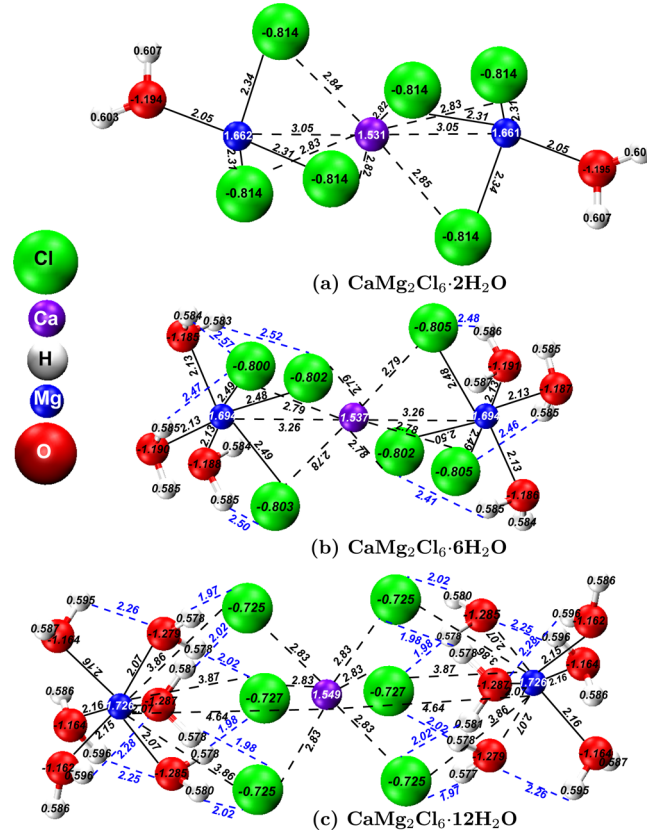


**Figure 2.** Molecular structure of several CM1 hydrates obtained from the GGA-DFT calculations. Bond lengths  $<2.5$  Å and  $>2.5$  Å are represented as continuous and broken lines, respectively. Blue broken lines represent intramolecular hydrogen bond lengths (in Å). The Bader atomic charges are also displayed.

hydrated state of Mg in CM1 ( $n = 12$ ) and  $\text{MgCl}_2$  ( $n = 6$ ) is similar.

In what concerns the Ca–Cl bonds, the central Ca atom is farther apart from the Cl atoms when compared with the two Mg atoms in CM1. Therefore, the Ca–Cl distance is observed to be less affected by hydration, as the Ca atom is shielded by the six chlorine atoms. The average Ca–Cl distance in all the hydrates of CM1 varies from 2.86 to 2.79 Å with  $n$  (Figure 2 and also Figures S1 and S2 of the Supporting Information).

Last, the optimized Ca–Mg distance in CM1 is found to increases from 3.00 to 4.64 Å as  $n$  increases from 0 to 12 (see Figure 3c). A sudden jump (0.56 Å) in the Ca–Mg interatomic distance happens as one passes from the lower hydrates to the higher ones ( $n$  increases from 6 to 8). A good agreement is observed between the theoretically determined geometry of  $\text{CM1}\cdot 12\text{H}_2\text{O}$  and that obtained from the experiments.<sup>29</sup>

The optimized structures (additionally, tables with all the bond lengths are provided in the Supporting Information) of the hydrates of CM2 are shown in Figure 4 (for hydration number  $n = 2, 6, 12$ ) and in Figures S3 and S4 of the Supporting Information (for hydration number  $n = 1, 4, 8, 10$ ). The average interatomic distance of the Ca–O pair in CM2 varies from 2.40 to 3.04 Å as  $n$  increases from 1 to 12 (see Figure 3a). Thus, the hydration strength decreases with  $n$  in the CM2 hydrates. In particular, we notice that successive hydration of the octahydrate of CM2 significantly reduces the hydration strength, as the Ca–O distance increases by 0.79 Å. The Ca–O

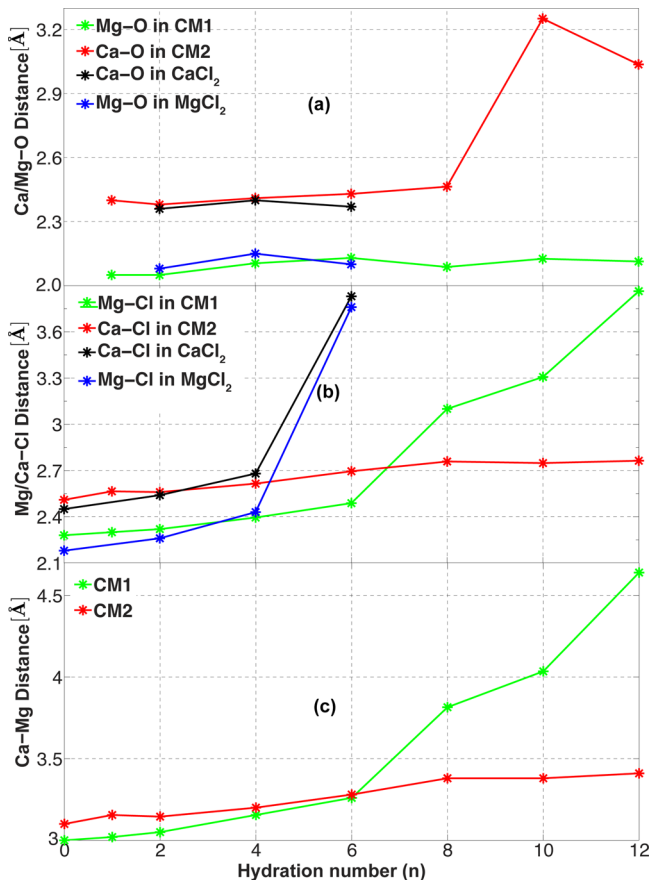


**Figure 3.** Comparison between several interatomic distances for the optimized geometry of the CM1 and CM2 hydrates and their elementary salt hydrates ( $\text{CaCl}_2$  and  $\text{MgCl}_2$ ), as a function of hydration number: (a)  $\text{Ca}/\text{Mg}-\text{O}$ , (b)  $\text{Mg}/\text{Ca}-\text{Cl}$ , and (c)  $\text{Ca}-\text{Mg}$  interatomic distances (in Å).

interatomic distance in  $\text{CaCl}_2$  hydrate is similar to the one in the CM2 hydrates of the same  $n$ .

The average  $\text{Ca}-\text{Cl}$  distance in CM2 gradually increases from 2.51 to 2.76 Å as  $n$  varies from 0 to 12 (see Figure 3b). The  $\text{Ca}-\text{Cl}$  interatomic distance in CM2 is 2.5–12.6% higher than the  $\text{Ca}-\text{Cl}$  distance in anhydrous  $\text{CaCl}_2$  (Figure 3b). The average  $\text{Ca}-\text{Cl}$  distance in  $\text{CaCl}_2$  gradually increases from 2.45 to 3.83 Å as  $n$  varies from 0 to 6. The  $\text{Ca}-\text{Cl}$  interatomic distance in the hexahydrated state of Ca in CM2 ( $n = 12$ ) and  $\text{CaCl}_2$  ( $n = 6$ ) differs by 1.07 Å. The hydrogen bonding between Cl and  $\text{H}_2\text{O}$  in CM2 hydrates is responsible for this difference.

The average  $\text{Mg}-\text{Cl}$  distance in all CM2 hydrates remains predominantly unperturbed with  $n$ . The central Mg atom and the Ca atoms have similar interatomic distance from the Cl atoms. The  $\text{Ca}-\text{Mg}$  interatomic distance gradually increases from 3.10 to 3.41 Å with increasing  $n$ , as shown in Figure 3c. The distance between the Cl and the central atom is predominantly unperturbed in both CM1 and CM2 hydrates. In the dodecahydrate of CM1 and CM2, the outer atoms (Mg/Ca) get hydrated with 6  $\text{H}_2\text{O}$  molecules and form a distorted octahedral structure (as shown in Figures 2c and 4c). These two distorted octahedron structures are connected via a bridge octahedral structure made from the central atom (Mg/Ca) and the Cl atom.

The Bader atomic charge on all the elemental atoms of CM1 and CM2 hydrates are shown in Figures 5 and 6 (additionally,

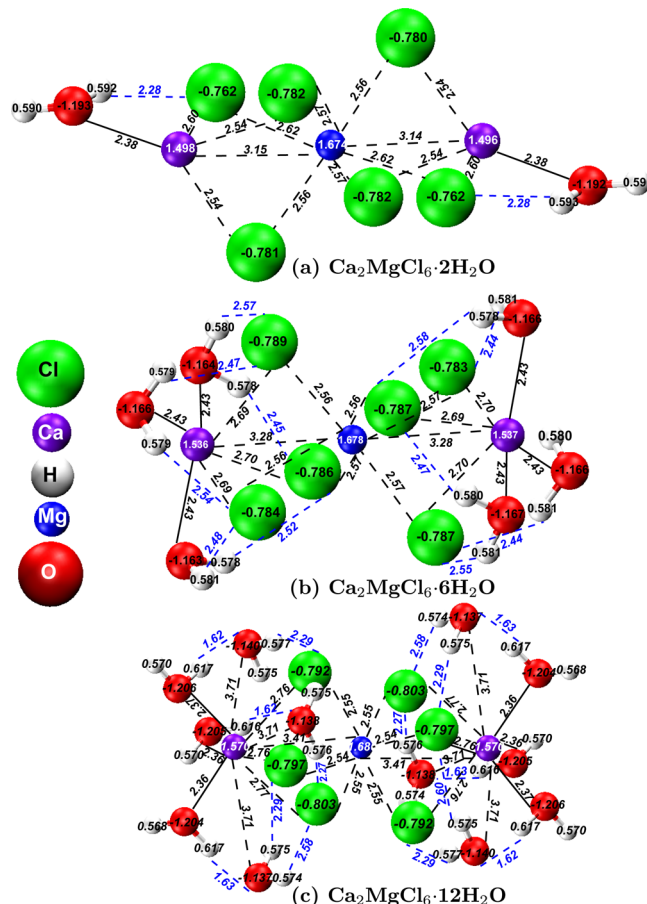


**Figure 4.** Molecular structure of several CM2 hydrates obtained from the GGA-DFT calculations. Bond lengths  $<2.5$  Å and  $>2.5$  Å are represented as continuous and broken lines, respectively. Blue broken lines represent intramolecular hydrogen bond lengths (in Å). The Bader atomic charges are also displayed.

tables with all the atom's Bader charge are provided in the Supporting Information). The electropositive charge on the Mg and Ca atoms in CM1 increases from 1.634 to 1.726 and from 1.528 to 1.549 as  $n$  increases from 0 to 12 (see Figures 2 and 5 and Figures S1 and S2 of the Supporting Information). The electropositive charges on Ca and Mg atoms in CM2 hydrates increase from 1.464 to 1.570 and from 1.672 to 1.680, respectively (see Figures 4 and 5 and Figures S3 and S4 of the Supporting Information). Comparatively, the electropositive charges on the Mg and Ca atoms in  $\text{MgCl}_2$  and  $\text{CaCl}_2$  hydrates increase from 1.621 to 1.762 and from 1.553 to 1.631, as  $n$  increases from 0 to 6. The charge modification with  $n$  on Mg/Ca atoms of the elementary salt hydrates is larger than in the chemical mixtures, because in the earlier case there is one Cl per Mg/Ca atom, while in the later case there are three Cl per Mg/Ca atom.

The atomic charge on the outer atoms (Mg in CM1 and Ca in CM2) increases more in comparison with the central atom (Ca in CM1 and Mg in CM2) after complete hydration. The outer atoms participate in the hydration process so their atomic charge modifies more than that of the central atoms in both CM1 and CM2 hydrates. The hydration strength of the outer atoms (Mg/Ca–O) progressively decreases with increasing  $n$  in both CM1 and CM2 hydrates. The electrostatic interactions play an important role in the hydration of the outer atoms.

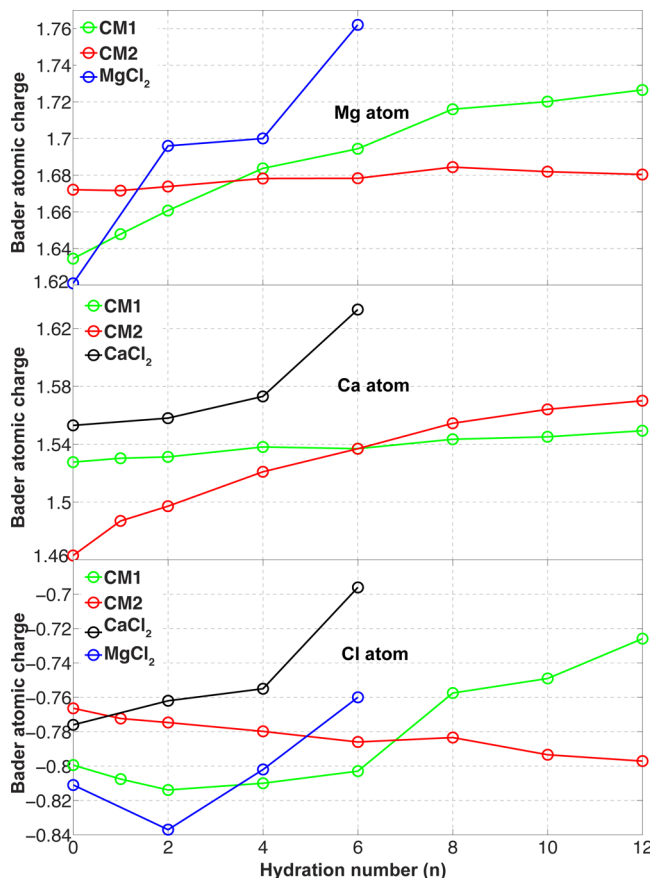


Figure 5. Variation of the calculated Bader atomic charge for the optimized geometry of the CM1 and CM2 hydrates as a function of hydration number.

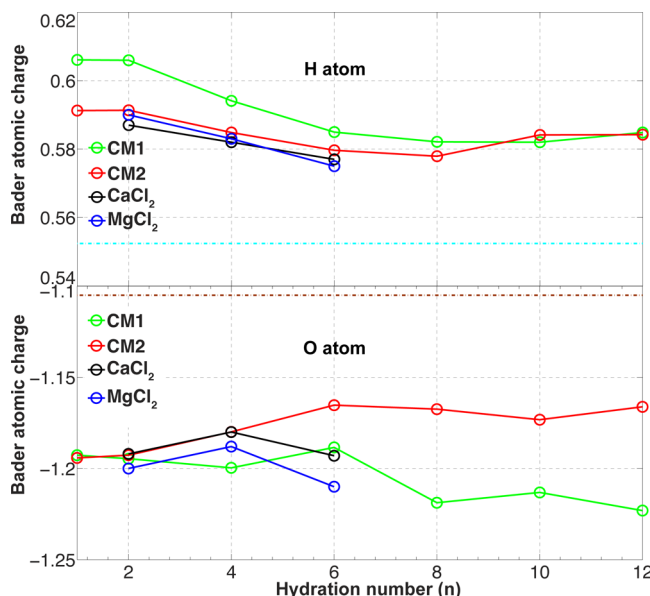


Figure 6. Variation of the calculated Bader atomic charge for the optimized geometry of the CM1 and CM2 hydrates as a function of hydration number. The cyan and brown dash-dot lines represent the charge on H and O in an isolated  $\text{H}_2\text{O}$  molecule.

In the CM1 hydrates, the average electronegative charge on the Cl atoms is continuously decreasing (from  $-0.814$  to  $-0.726$ ), while it continuously increases (from  $-0.775$  to

$-0.797$ ) in the CM2 hydrates with increasing  $n$  from 2 to 12 (see Figure 5). There is a small sudden jump of 0.045 observed as  $n$  changes from 6 to 8 in the CM1 hydrates. Comparatively, in the elementary salts, the average electronegative charge on the Cl atoms is continuously decreasing (from  $-0.781$  to  $-0.760$ ) in the  $\text{MgCl}_2$  hydrates and, as well, in the  $\text{CaCl}_2$  hydrates (from  $-0.776$  to  $-0.696$ ), when increasing  $n$  from 0 to 6. The Cl charge in the lower hydrates of CM1 has a similar trend to the Cl charge in  $\text{MgCl}_2$  hydrates.

The charge on the H atoms decreases with the hydration number for both CM1 and CM2 hydrates, as shown in Figure 6. The magnitude of the atomic charge on the H atoms in CM1 and CM2 hydrates is always higher than the H charge of  $\text{H}_2\text{O}$ , as shown by the cyan dotted line in Figure 6. In CM1, the Mg atoms get hydrated, while in CM2, the Ca atoms get hydrated. Owing to the electronic charge caused by the difference in their electronegativity, the electronic charge on the H of the lower hydrates of CM1 is found to be higher than the electronic charge on the H of the lower hydrates of CM2.

The magnitude of the atomic charge present on the O atoms in the CM1 and in the CM2 hydrates is higher than the O charge present in the  $\text{H}_2\text{O}$  molecule (brown dotted line in Figure 6). We also observe that the O charge in CM1 increases in magnitude following the hydration, while it decreases for the CM2 hydrates. For the CM1 hydrates we also notice the presence of a small, but sudden jump, for the O charge as  $n$  increases from 6 to 8.

The presence of a small sudden jump in the O and Cl atomic charges, as well as in the Mg–Cl and Mg–Ca distances, as  $n$  changes from 6 to 8, occurs because in the CM1 hydrates up to hexahydrate, the  $\text{H}_2\text{O}$  molecule is attached to the outer region of the Mg atoms. Successive addition of two  $\text{H}_2\text{O}$  molecules results in their positioning in the inner region between Mg and Cl atoms (compare Figures S1 and S2 from Supporting Information). These  $\text{H}_2\text{O}$  molecules push the Cl atoms, and acts also on the central Ca atom. This seems to be the reason for the sudden jump. In the CM2, the interatomic distance between the Ca–Cl and the Ca–O is larger than the Mg–Cl and the Mg–O distance in the CM1. Thus, such a sudden jump is not observed in the CM2 hydrates.

The atomic charge distribution on O, H, Mg, and Ca suggests that the electrostatic interactions are playing a major role in the stability and the hydration of these hydrates.

As the main focus of the present study is to evaluate the effect of the chemical mixing of  $\text{CaCl}_2$  and  $\text{MgCl}_2$  hydrates on the thermolysis, under various operating conditions, and to compare this with the values obtained for the elementary salt hydrates. In this direction, we have computed the vibrational spectra for the chemical mixtures of the salt hydrates in order to further calculate the Gibbs free energies. From the analysis of the vibrational spectra, we observe that the O–H pair contributes to the most energetic peak in the vibrating spectra of the chemical mixture. The theoretical spectra for the O–H symmetric bond stretching, for the O–H asymmetric stretching and for the H–O–H angle bending obtained from the GGA-DFT spectrum in the various hydrates of the chemical mixture is shown in Figure 7. We compared this with the theoretical vibrational spectrum obtained for an isolated  $\text{H}_2\text{O}$  molecule.<sup>57,58</sup> A careful examination of parts a and b of Figure 7 reveals that the vibration spectra of the O–H bond stretching and the H–O–H angle bending of the chemical mixture hydrates are somewhat different than the vibrational spectra of the isolated  $\text{H}_2\text{O}$  molecule. We observe a red-shift in the O–H

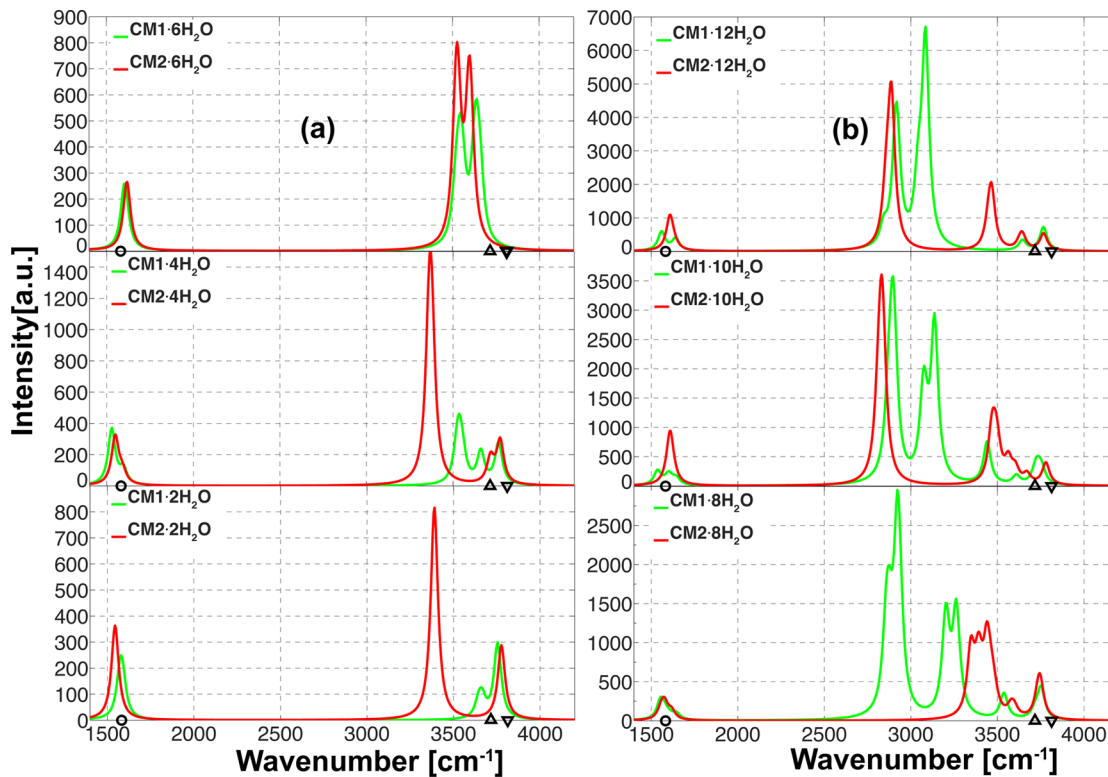


**Figure 7.** GGA-DFT computed vibrational frequencies of O–H bond and H–O–H angle present in various chemical mixture hydrates: (a) lower hydrates and (b) higher hydrates. The vibrational spectra are compared with the spectra of an isolated H<sub>2</sub>O molecule, marked with (○) H–O–H bending, (△) O–H symmetric stretching, and (▽) O–H asymmetric stretching.

bond stretching and H–O–H angle bending, when comparing with the isolated H<sub>2</sub>O molecule for all the chemical mixtures hydrates except CM1·2H<sub>2</sub>O. For CM1·2H<sub>2</sub>O, the location of the O–H and H–O–H peaks is similar to that found in the isolated H<sub>2</sub>O molecule, due to the lack of hydrogen bonds formation. The electrons of O atom shared in hydration and hydrogen bond formation impairs the O–H bond strength, thus resulting in the red-shift of the O–H bonds present in the chemical mixture hydrates. The extent of the red-shift depends on the strength variation of the O–H bond, which is affected by hydration strength and the hydrogen bonding interactions in the chemical mixture hydrates. The strength of the symmetric O–H bond in the CM2 hydrates is lower than that found in CM1 (except octahydrate). There are few very strong O–H–O and O–H–Cl type hydrogen bonds observed in higher hydrates in CM1 and CM2; thus, few of the peaks of the O–H bond get elongated, resulting in a large red-shift.

**Bonding Indicators in CM1 and CM2 Hydrates.** To investigate the bonding proclivities between distinct atomic pairs, we have calculated the integrated crystal orbital Hamiltonian population (ICOHP), the integrated crystal orbital overlap population (ICOOP), the electron density (ED), and the Laplacian ( $L$ ) at relevant bond critical points (BCPs) (see Figure 8 for a model of Bader topology), as well as the bond orders (BO) for several CM1 and CM2 hydrates. This is important as the strength of Mg/Ca–Cl and Mg/Ca–O pairs describe the dehydration, hydrolysis behavior and the stability of the chemical mixtures. The ICOHP/ICOOP, ED/ $L$  at BCPs and BO of the lower hydrates are given in Table 1. The “Mg/Ca–O” notation in Table 1 refers to the Mg–O pair in CM1 hydrates and to the Ca–O pair in CM2 hydrates. The Bader topological analysis of the higher hydrates for the

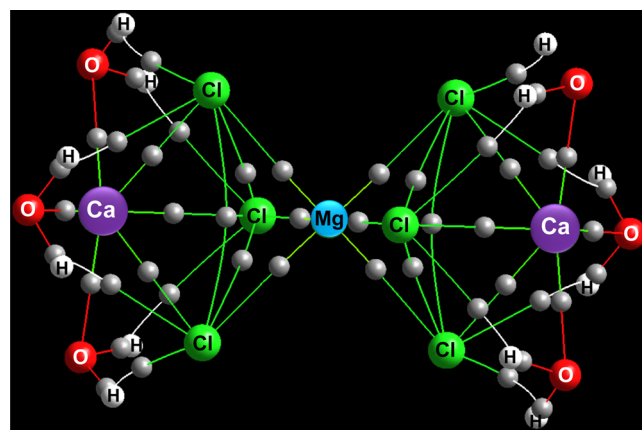


**Figure 8.** Bond critical points (BCPs) in CM2·6H<sub>2</sub>O. Small gray spheres represent the BCP.

chemical mixtures is computationally demanding. Thus, the Bader topological analysis (ED/ $L$ ) is only carried out for the lower hydrates.

The bond order of the Mg–Cl pair in CM1 hydrates decreases with increasing  $n$ , and reduces by 46.9% as  $n$  increases from 0 to 6. The ED follows the same trend as it reduces by 38.8% as  $n$  increases from 0 to 6 (see Table 1). This suggests that the covalent contribution to the Mg–Cl bond strength is decreasing with increasing hydration. The positive sign of the Laplacian suggests the presence of an ionic bonding contribution, which is to be expected due to the difference in electronegativity between Mg and Cl. With increase in hydration the ionic bond strength is found to decrease by 41.3% as  $n$  increases from 0 to 6. Thus, the hydration of Mg

**Table 1.** Bond Order (BO), Electron Density (ED) and Laplacian ( $L$ ) at Bond Critical Points (BCPs), Integrated Crystal Orbital Hamilton Population (ICOHP), and Integrated Crystal Orbital Overlap Population (ICOOP) Values in Lower Hydrates of CM1 and CM2<sup>a</sup>

Molecule	Bond pair	BO	BO	ED/L	ED/L	ICOOP/ICOHP	ICOOP/ICOHP
		CM1	CM2	CM1	CM2	CM1	CM2
Anhyd	Ca-Cl	0.197	0.368	0.163/1.939	0.332/3.615	0.00/-0.553	0.00(-0.905)
2W	Ca-Cl	0.201	0.354	0.168/2.043	0.312/3.541	0.0/-0.564	0.00/-0.860
2W	Ca-Cl	0.206	0.357	0.163/2.003	0.310/3.532	0.0/-0.564	0.00/-0.860
2W	Ca-Cl	0.204	0.276	0.167/2.036	0.273/3.132	0.0/-0.570	0.02/-0.839
4W	Ca-Cl	0.208	0.321	0.170/2.129	0.241/2.903	0.00/-0.617	0.00/-0.675
4W	Ca-Cl	0.211	0.250	0.173/2.158	0.286/3.333	0.01/-0.632	0.01/-0.933
4W	Ca-Cl	0.220	0.274	0.181/2.278	0.261/3.083	0.00/-0.653	0.02/-0.848
6W	Ca-Cl	0.218	0.221	0.179/2.273	0.216/2.659	0.01/-0.692	0.02/-0.747
6W	Ca-Cl	0.219	0.221	0.180/2.278	0.218/2.686	0.01/-0.693	0.02/-0.748
6W	Ca-Cl	0.218	0.218	0.179/2.272	0.218/2.682	0.01/-0.698	0.02/-0.741
Anhyd	Mg-Cl	0.414	0.204	0.312/5.211	0.163/2.415	0.07/-1.243	0.03/-0.683
2W	Mg-Cl	0.385	0.214	0.295/4.981	0.169/2.533	0.08/-1.384	0.07/-0.927
2W	Mg-Cl	0.381	0.212	0.290/4.873	0.171/2.567	0.06/-1.167	0.05/0.821
2W	Mg-Cl	0.341	0.183	0.273/4.570	0.143/2.114	0.08/-1.394	0.04/-0.731
4W	Mg-Cl	0.313	0.194	0.243/4.025	0.155/2.332	0.07/-1.197	0.06/-0.887
4W	Mg-Cl	0.260	0.196	0.256/4.276	0.175/2.652	0.07/-1.094	0.04/-0.769
4W	Mg-Cl	0.289	0.194	0.223/3.625	0.156/2.322	0.08/-1.303	0.05/-0.826
6W	Mg-Cl	0.219	0.204	0.192/3.073	0.162/2.450	0.08/-1.082	0.04/-0.825
6W	Mg-Cl	0.220	0.204	0.192/3.059	0.164/2.496	0.08/-1.047	0.04/-0.824
6W	Mg-Cl	0.220	0.202	0.190/3.032	0.164/2.486	0.07/-1.021	0.04/-0.820
2W	Mg/Ca-O	0.295	0.214	0.285/6.395	0.227/3.920	0.02/-0.821	0.0/-0.424
4W	Mg/Ca-O	0.261	0.186	0.274/6.115	0.228/3.882	0.02/-0.739	0.00/-0.385
4W	Mg/Ca-O	0.208	0.209	0.241/5.007	0.231/3.528	0.02/-0.583	0.00/-0.421
6W	Mg/Ca-O	0.209	0.179	0.249/5.154	0.234/3.500	0.01/-0.570	0.00/-0.379
6W	Mg/Ca-O	0.209	0.179	0.249/5.153	0.234/3.504	0.01/-0.583	0.00/-0.378
6W	Mg/Ca-O	0.209	0.179	0.249/5.169	0.234/3.499	0.02/-0.621	0.00/-0.378

<sup>a</sup>The results for the CM1 are depicted with green color, while the ones for the CM2 are shown with red color.

reduces the bond strength with the Cl atoms. As a consequence of the hydration of the Mg atoms, the Cl atoms are pushed toward the central Ca in CM1, resulting in a slightly increased strength for the Ca-Cl bond with increase in  $n$ . This is confirmed by the increasing values of BO and ED ( $\approx 10\%$ ) and  $L$  ( $\approx 17\%$ ) for the Ca-Cl bond as  $n$  grows from 0 to 6 in CM1 hydrates (refer to Table 1).

The hydration strength (Mg-O pair) in CM1 hydrates is found to decrease with increasing  $n$ . The Mg-O bond order drops-down 29.14% by increasing  $n$  from 2 to 6 (see Table 1). ED and  $L$  at BCP for Mg-O pairs also confirm the same trend and drops-down by 12.6% and 19.3%, respectively, with increasing  $n$  from 2 to 6.

In the CM2 hydrates, the bond order of the Ca-Cl pair (the equivalent of the Mg-Cl pair in CM1 hydrates) decreases with 40.2% with increasing  $n$  from 0 to 6. This is similar to the 46.9% decrease for the Mg-Cl pair in CM1. The ED and  $L$  also reduce by 34.6% and 26.1% for the Ca-Cl bond, as  $n$  increases from 0 to 6. Thus, the higher hydration reduces the strength for the Ca-Cl bond. As we found for Mg-Cl bond, the Ca-Cl bond has also a significant ionic character, evident from the positive sign of  $L$ . As the size of Ca is larger than that of Mg, Cl atoms get only marginally pushed toward the central Mg atom following the hydration of the Ca atoms in CM2. Hence, the strength of the Mg-Cl bond remains unaltered by hydration. This is different from the CM1 case, where increase in hydration leads to increase in proximity for the Ca and Cl atoms, and therefore to stronger Ca-Cl bonds. The hydration strength (Ca-O pair) in CM2 hydrates decreases with increasing  $n$ . The Ca-O bond order and Laplacian drop-

down by 16.35% and by 10.7%, respectively, with  $n$  increasing from 2 to 6 (see Table 1).

In general, similar trends are observed for all the investigated bonds when looking at their COHP plots and average ICOHP values (see Figure 9 and Table S8 of Supporting Information).

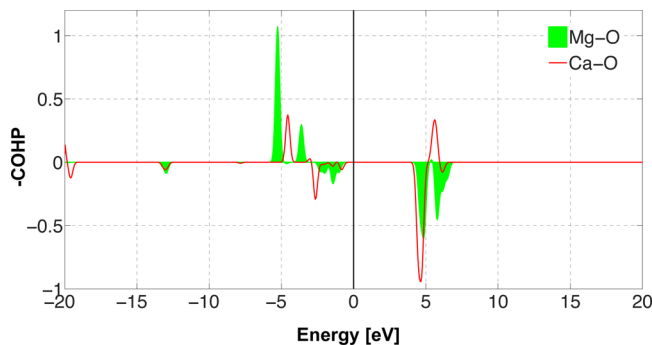


**Figure 9.** COHP plot for the Mg-O and Ca-O bonds present in CM1·6H<sub>2</sub>O and in CM2·6H<sub>2</sub>O, respectively. The “0” value on the X-axis separates occupied from unoccupied states. The “0” value on the Y-axis separates bonding (positive values) from antibonding (negative values) states.

From the COHP plots of Mg-O (in CM1·6H<sub>2</sub>O) and Ca-O (in CM2·6H<sub>2</sub>O), we can also distinguish the bonding, antibonding and nonbonding domains associated with these bonds. We observed that the Mg-O bond has more occupied bonding contributions than the Ca-O bond, the latter one having essentially equally occupied bonding and antibonding

contributions. This is also confirmed by their corresponding ICOHP and ICOOP values (when comparing ICOHP values between different systems, care has to be taken as the reference values for the absolute number are not fixed).

In order to compare the strength of Ca/Mg–Cl and Ca/Mg–O pairs between the elementary hydrates and the chemical mixture hydrates we have calculated also the bond order, ED, and  $L$  at BCP for the  $\text{CaCl}_2$  and  $\text{MgCl}_2$  elementary hydrates. The obtained values for the elementary salt hydrates are given in Table S9 of the *Supporting Information*. The bond order of Mg–Cl in anhydrous CM1 is 33.4% lower than in anhydrous  $\text{MgCl}_2$ . Similarly smaller values, by 20.8% and by 23.5%, are obtained also for the ED and  $L$  of the Mg–Cl in anhydrous CM1 when compared to the Mg–Cl in anhydrous  $\text{MgCl}_2$ . For the hydrate, the bond order of Mg–Cl pair in  $\text{CM1}\cdot\text{2H}_2\text{O}$  is similar to that of  $\text{MgCl}_2\cdot\text{2H}_2\text{O}$ . The ED and  $L$  of the Mg–Cl pair in  $\text{CM1}\cdot\text{2H}_2\text{O}$  are however slightly lower (by 7%) than that of the  $\text{MgCl}_2\cdot\text{2H}_2\text{O}$ . The bond order of the Mg–Cl pair in  $\text{CM1}\cdot\text{4H}_2\text{O}$  is 21.2% higher than that in the  $\text{MgCl}_2\cdot\text{4H}_2\text{O}$ , and in  $\text{CM1}\cdot\text{6H}_2\text{O}$  is 44 times higher than that in the  $\text{MgCl}_2\cdot\text{6H}_2\text{O}$  (see Table 1 and Table S9 of *Supporting Information*). The ED and  $L$  of the Mg–Cl pair in  $\text{CM1}\cdot\text{4H}_2\text{O}$  are approximately 10% higher than those in the  $\text{MgCl}_2\cdot\text{4H}_2\text{O}$ . No ionic interaction is observed between Mg–Cl pair in  $\text{MgCl}_2\cdot\text{6H}_2\text{O}$ . The bond order of Mg–O in CM1 di-, tetra-, and hexahydrates is 18.5%, 22.8% and 16.1% higher than in the di-, tetra-, and hexahydrates of  $\text{MgCl}_2$ , respectively. Similarly, the ED of Mg–O in CM1 di-, tetra-, and hexahydrates are 6.3%, 11.5%, and 0.4% higher than in the di-, tetra-, and hexahydrates of  $\text{MgCl}_2$ , respectively. The Laplacians match the same trends, with the values for the Mg–O bond in the di-, tetra-, and hexahydrate of CM1 being with 3.5%, 11.9% and 5.2% higher than in the corresponding hydrates of  $\text{MgCl}_2$ . Thus, comparative bond order analysis reveals that the strength of Mg–Cl and Mg–O bonds in CM1 hydrates is stronger than that in the  $\text{MgCl}_2$  hydrates.

The bond order of Ca–Cl in anhydrous and dihydrates of CM2 is 25.9%, 10.6% lower than in the anhydrous and dihydrate of  $\text{CaCl}_2$ , respectively. The ED of Ca–Cl in anhydrous and dihydrates of CM2 are also 12.40%, and 4.1% lower than in the anhydrous and dihydrate of  $\text{CaCl}_2$ , respectively. The Laplacians follow the same trend showing a 14.8% and 5.2% smaller value than in the anhydrous and dihydrate of  $\text{CaCl}_2$ . The BO, ED, and  $L$  of Ca–Cl pair in  $\text{CM2}\cdot\text{4H}_2\text{O}$  are however 24.1%, 26.3%, and 21.2% higher than in the  $\text{CaCl}_2\cdot\text{4H}_2\text{O}$ . The BO of Ca–Cl pair in  $\text{CM2}\cdot\text{6H}_2\text{O}$  is 24.4 times higher than in the  $\text{CaCl}_2\cdot\text{6H}_2\text{O}$  (see Tables 1 and Table S9 of the *Supporting Information*).

The BO of Ca–O in  $\text{CM2}\cdot\text{2H}_2\text{O}$  is found to be 0.9% lower than in the  $\text{CaCl}_2\cdot\text{2H}_2\text{O}$ . The bond orders of Ca–O in CM2 tetra- and hexa-hydrates are 5.6% and 2.3% higher than in tetra- and hexahydrates of  $\text{CaCl}_2$ , respectively. Thus, comparative bond order analysis reveals that the strength of Ca–Cl and Ca–O bond in  $\text{CM2}\cdot\text{2H}_2\text{O}$  is weaker than in  $\text{CaCl}_2\cdot\text{2H}_2\text{O}$  hydrates. The Ca–Cl and Ca–O bonds in tetra- and hexahydrates of CM2 are however stronger than the corresponding bonds from the tetra- and hexahydrates of  $\text{CaCl}_2$ .

**Enthalpy Change in Thermolysis.** Hydrolysis is usually observed in lower hydrates of  $\text{MgCl}_2$  hydrates ( $\text{MgCl}_2\cdot\text{H}_2\text{O}$  and  $\text{MgCl}_2\cdot\text{2H}_2\text{O}$ ).<sup>59</sup> The proton transfer is an important step in the hydrolysis of chloride-based hydrates.<sup>34</sup> To quantify the comparative hydrolysis resistance among  $\text{MgCl}_2$  and  $\text{CaCl}_2$  hydrates, we have calculated the enthalpy change in proton

removal for  $\text{CaCl}_2\cdot\text{2H}_2\text{O}$  and  $\text{MgCl}_2\cdot\text{2H}_2\text{O}$ . The enthalpy change is obtained by gradually increasing the O–H interatomic distance. The enthalpy change of the proton dissociation in  $\text{MgCl}_2\cdot\text{2H}_2\text{O}$  is found to be 19.55 kcal/mol, and 33.73 kcal/mol in  $\text{CaCl}_2\cdot\text{2H}_2\text{O}$ . The proton transfer is thus less energy favorable in  $\text{CaCl}_2\cdot\text{2H}_2\text{O}$  when compared with  $\text{MgCl}_2\cdot\text{2H}_2\text{O}$ . This suggests that  $\text{CaCl}_2\cdot\text{2H}_2\text{O}$  is more resistant to hydrolysis than  $\text{MgCl}_2\cdot\text{2H}_2\text{O}$ . This reiterates our previous DFT results, which suggest that  $\text{CaCl}_2$  hydrates are more hydrolysis resistant than  $\text{MgCl}_2$  hydrates.<sup>52</sup> This is the fundamental reason to explore the effect of chemical mixing of  $\text{CaCl}_2$  hydrates and  $\text{MgCl}_2$  hydrates on their hydrolysis resistance.

The enthalpy change in dehydration, hydrolysis, and binding of  $\text{H}_2\text{O}$  to a chemical mixture of salt, as defined by eqs 3, 4, and 5 are shown in Figure 10. The dehydration enthalpy

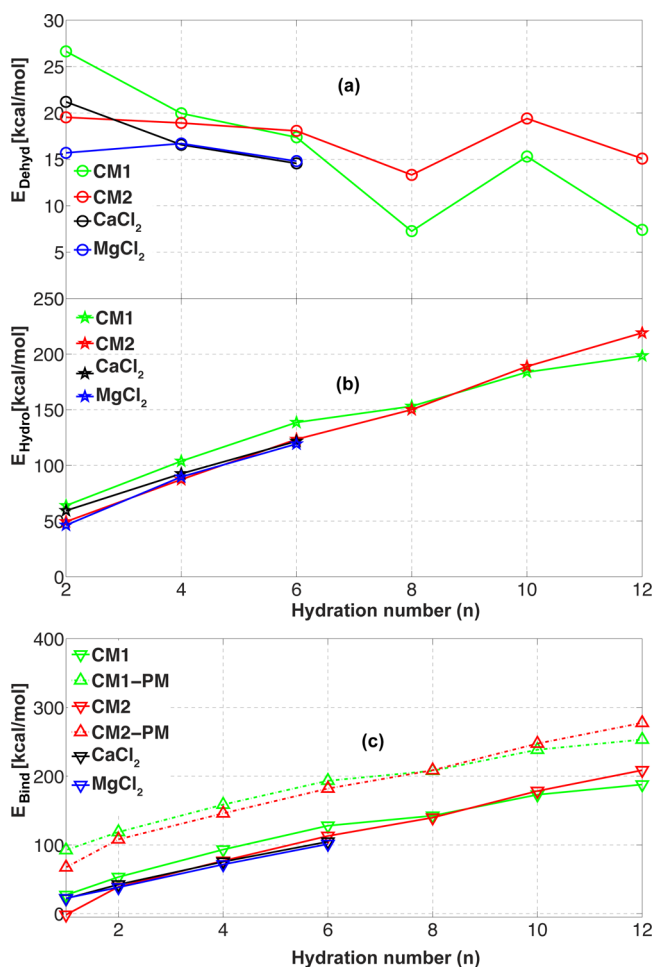


**Figure 10.** Enthalpy change during (a) dehydration per mole of  $\text{H}_2\text{O}$ , (b) hydrolysis, and (c) binding of various chemical mixture hydrates per mole of salt studied. The black and blue solid lines represent the enthalpy change in  $\text{CaCl}_2$  and  $\text{MgCl}_2$  hydrates, respectively. The dotted line (-PM) from panel c represents the enthalpy change considering the physical mixture.

monotonically decreases with  $n$  until octahydrate then increases for decahydrate and decreases again for dodecahydrate in both CM1 and CM2 hydrates. This indicates that the dehydration process becomes energetically favorable with the increase of  $n$  until octahydrate for both CM1 and CM2 hydrate. In CM1 hydrates,  $\text{H}_2\text{O}$  molecules are attached to Mg, and therefore the change in the dehydration enthalpy with  $n$  is more than for the

Ca hydrated CM2 hydrates. From Figure 10a, we observed that a crossover in dehydration enthalpy between CM1 and CM2 hydrates appears for  $n = 6$ . The bonding indicator (ED) suggests that the hydration strength of Mg–O is decreasing with  $n$  in CM1, while the hydration strength is only marginally affected by the increase of  $n$  in CM2. This explains the crossover. We also observe that the dehydration enthalpies for octa- and dodeca-hydrates of CM1 are less than 10 kcal/mol. Thus, these hydrates are not stable at room temperature. Comparing the dehydration enthalpy of chemical mixtures with that of their elementary salt hydrates, we observed that the chemical mixtures have larger enthalpies than the elementary hydrates (except for  $\text{CaCl}_2 \cdot 2\text{H}_2\text{O}$ ).

The enthalpy change in hydrolysis of CM1 and CM2 hydrates monotonically increases with  $n$  as shown in Figure 10b. This indicates that the hydrolysis process becomes energetically more difficult with increasing  $n$ . The hydrolysis enthalpy of CM1 lower hydrates is with  $\approx 15$  kcal/mol higher than that of CM2 lower hydrates. We observe again a crossover in enthalpy change of hydrolysis at  $n = 8$  for CM1 and CM2 hydrates. The Mg–Cl distance and Cl Bader charge have a crossover at hydration  $n = 8$  for CM1 (see Figures 3c and 5c). This might be a plausible reason for the crossing. Comparing the hydrolysis enthalpy for CM1, CM2 and elemental hydrates, we notice that the hydrolysis enthalpy of CM2 hydrates matches very close that of the  $\text{MgCl}_2$  hydrates.

The enthalpy change in binding of  $\text{H}_2\text{O}$  to the salt mixture is found to increase with  $n$  as shown in Figure 10c. The increase in the binding enthalpy with successive hydration of the  $\text{H}_2\text{O}$  molecules decreases with  $n$  for both CM1 and CM2 hydrates. The binding enthalpy of the monohydrate of CM2 is negative and close to 0 kcal/mol, thus binding of one  $\text{H}_2\text{O}$  to CM2 is energetically unfavorable. Hydrolysis process becomes energetically challenging with the increase in  $n$ . The binding enthalpy of CM1 lower hydrates is with  $\approx 15$  kcal/mol higher than that of CM2 lower hydrates. A crossover in binding enthalpy is also observed for  $n = 8$ . The same reason for structural change at  $n = 8$  in CM1 hydrates is assumed to be the plausible cause. Comparing with the elementary salt hydrates, the binding enthalpy of the chemical mixtures is found to be higher (except for the CM2 monohydrate). The binding enthalpy of the chemical mixture has been also compared with the binding enthalpy of the physical mixture (-PM, dotted line in Figure 10c) of same stoichiometric ratio. The binding enthalpy of the chemical mixture is lower than that of the physical mixture. The lowering in binding enthalpy can be explained by the fact that a fraction of binding enthalpy of physical mixture is utilized in chemical rearrangement of salt to form the chemical mixture.

**Thermodynamic Study of Chemical Mixture.** To explore the effect of chemical mixing on the thermolysis (dehydration/hydrolysis) of salt hydrate mixtures, we have obtained the equilibrium compositions (partial pressure) of products formed during the thermolysis. The equilibrium compositions are obtained from thermodynamics by equating  $\Delta G$  to zero. The Gibbs free energy of each reactant and product is obtained from atomistic GGA-DFT calculations.<sup>31,52</sup> In seasonal heat storage systems, the typical operating temperature varies between 300 and 500 K and the partial pressure of water ( $p_{\text{H}_2\text{O}}$ ) varies from  $10^{-3}$  to 1 atm.<sup>4</sup> In the present study, we have chosen the partial pressure of water ( $p_{\text{H}_2\text{O}}$ ), the partial pressure of HCl ( $p_{\text{HCl}}$ ) and the temperature

( $T$ ) as controlling variables while the partial pressures of the salt hydrates are kept constant (1 atm).

**Dehydration Reaction of Salt Hydrates Mixture.** The water vapor pressure and reaction temperature affect the reversible endothermic dehydration of the chemical mixture of  $\text{MgCl}_2$  and  $\text{CaCl}_2$  hydrates. To understand their effect on the dehydration reaction of CM1 and CM2 hydrates, the equilibrium product compositions of dehydration are investigated in the temperature range of 100 to 600 K and an arbitrary water vapor pressure ( $p_{\text{H}_2\text{O}}$ ) in the range of 0.001–1 atm. This temperature range is chosen to examine all the dehydration reactions of CM1 and CM2 hydrates for seasonal heat storage. The dehydration characteristics of the elementary salt hydrates of  $\text{CaCl}_2$  and  $\text{MgCl}_2$ , under similar conditions and DFT formalism, have been previously found to be in agreement with the corresponding experiments.<sup>31,52</sup>

The equilibrium temperature-vapor pressure obtained from the dehydration reactions of the higher hydrates of both  $\text{CM1}\cdot n\text{H}_2\text{O}$  and  $\text{CM2}\cdot n\text{H}_2\text{O}$  ( $n = 8, 10, 12$ ) is shown in Figure S10a of Supporting Information. The dodeca- and octa-hydrates of CM1 dehydrate at very low temperature (<200 K), thus they are unstable at room temperature. This behavior of CM1 hydrate is consistent with their low change in dehydration enthalpy (<10 kcal/(mol K)) shown in Figure 10a. The decahydrate of CM1 dehydrates in the temperature range of 290 to 408 K. The higher hydrates of CM2 dehydrate in the temperature range of 297 to 551 K as shown in Figure S10a of Supporting Information. The higher hydrates of CM2 have higher dehydration enthalpy (>10 kcal/(mol K)) than the CM1 higher hydrates, as shown in Figure 10a.

The equilibrium product composition of lower hydrates of  $\text{CM1}\cdot n\text{H}_2\text{O}$  and  $\text{CM2}\cdot n\text{H}_2\text{O}$  ( $n = 2, 4, 6$ ) is shown in Figure 11. These equilibrium curves are compared with their analogous for hydrates of  $\text{CaCl}_2$  and  $\text{MgCl}_2$  of same  $n$ . The dehydration temperatures for hexa- and tetrahydrate of CM1 and CM2 are higher than those of the hexa- and tetrahydrates of  $\text{CaCl}_2$  and  $\text{MgCl}_2$ . The equilibrium partial vapor pressure ( $p_{\text{H}_2\text{O}}$ ) of 1 atm is observed at 478 and 408 K for  $\text{CM1}\cdot 6\text{H}_2\text{O}$  and  $\text{CM2}\cdot 6\text{H}_2\text{O}$ , respectively. For the elementary salt hydrates the equivalent temperature for  $\text{CaCl}_2\cdot 6\text{H}_2\text{O}$  and  $\text{MgCl}_2\cdot 6\text{H}_2\text{O}$  is 350 and 390 K as shown in Figure 11a. For the tetrahydrate the equilibrium temperature at  $p_{\text{H}_2\text{O}}$  of 1 atm is obtained at 576, 626, 490, and 374 K for  $\text{CM1}\cdot 4\text{H}_2\text{O}$ ,  $\text{CM2}\cdot 4\text{H}_2\text{O}$ ,  $\text{CaCl}_2\cdot 4\text{H}_2\text{O}$ , and  $\text{MgCl}_2\cdot 4\text{H}_2\text{O}$ , respectively. The equivalent temperatures for  $\text{CM1}\cdot 2\text{H}_2\text{O}$ ,  $\text{CM2}\cdot 2\text{H}_2\text{O}$ ,  $\text{CaCl}_2\cdot 2\text{H}_2\text{O}$  and  $\text{MgCl}_2\cdot 2\text{H}_2\text{O}$  are 1106, 704, 895, and 733 K, respectively.

The dehydration characteristics of the chemical mixture are different than that of their elementary component salt hydrates and it depends on the hydration strength. In the higher hydrates of the chemical mixture ( $n = 8–12$ ), CM2 dehydrates at a greater temperature than CM1, while in lower hydrates, this is reversed (except for tetrahydrate). Chemical mixing increases the dehydration temperature range by 30, 72, and 182 K for hexa-, tetra-, and dihydrates of CM1, when compared with analogous elementary  $\text{MgCl}_2$  hydrates. It increases the dehydration temperature range by 63 K and decreases by 123 K for hexa- and tetrahydrate of CM2, when compared with analogous elementary  $\text{CaCl}_2$  hydrates. The chemical mixing can be used therefore to increase/decrease the temperature operation range of TCM based seasonal heat storage systems. On the basis of the fact that the chemical mixing generally increases the temperature interval for the dehydration, CM1-

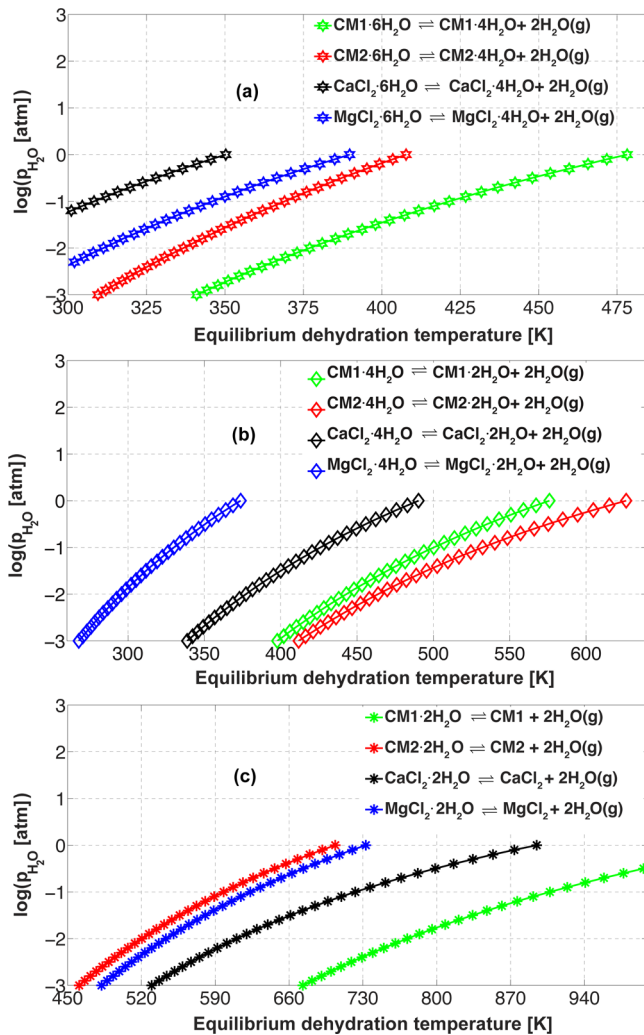


**Figure 11.** Equilibrium product concentrations for the dehydration reactions of lower hydrates of CM1 and CM2, and their comparison with the analogous  $CaCl_2$  and  $MgCl_2$  hydrates at various temperatures and constant partial pressure of hydrate,  $p_o = 1$  atm.

$nH_2O$  and  $CM2 \cdot nH_2O$  can be considered as better candidates than their elementary salts for efficient heat storage, from the dehydration point of view.

**Hydrolysis Reaction of Salt Hydrates.** Hydrolysis is an undesirable side reaction in thermolysis of chloride-based salt, which produces HCl and  $H_2O$ . Hydrolysis starts at a higher temperature than dehydration as the enthalpy change in hydrolysis is much higher than the enthalpy change in dehydration, as depicted in Figure 10. The hydrolysis characteristics for the elementary salt hydrates of  $CaCl_2$  and  $MgCl_2$ , under similar DFT formalism, have been investigated previously and found to be in good agreement with the experiments.<sup>31,52</sup> To understand the effect of temperature and partial pressure of the products ( $p_{HCl}$ ,  $p_{H_2O}$ ) on hydrolysis, we have varied the concentrations of either of the reaction products while keeping the concentration of the other product fixed. The equilibrium temperature is varied from 300 K–800 K at constant HCl pressure (0.001 atm). To mimic a very slow hydrolysis rate, low fixed HCl pressure ( $p_{HCl} = 0.001$  atm) is chosen, which gives low HCl pressure gradient. Such low concentrations of HCl could be chosen as the safety limit for the seasonal heat storage system.

The equilibrium hydrolysis curve of higher hydrates of chemical mixture ( $CM1/CM2 \cdot nH_2O$ ,  $n = 8, 10, 12$ ) at fixed  $p_{HCl}$  and fixed  $p_{H_2O}$  is depicted in Figure S10, parts b and c, of the Supporting Information, respectively. The onset temperature of hydrolysis to attain  $p_{H_2O}$  of 0.001 atm at fixed HCl pressure ( $p_{HCl} = 0.001$  atm) is 315 K, 351 and 366 K for dodeca-, deca- and octa-hydrate of CM1, respectively, as shown in Figure S10b. The corresponding temperatures for CM2 hydrates are 382 K, 380 and 381 K. The temperature to attain  $p_{HCl}$  of 0.001 atm are 345 K, 384 and 400 K at fixed  $p_{H_2O}$  of 0.01 atm for dodeca-, deca-, and octahydrate of CM1 (see Figure S10c of Supporting Information). The corresponding temperatures for the analogous CM2 hydrates are 421.5, 418.8, and 419.5 K. The dodeca- and octa-hydrates of CM1 are not stable at room temperature, so their hydrolysis behavior can be ignored. The onset temperature of hydrolysis is greater in higher hydrates of CM2 than in CM1 hydrates, in both investigated conditions (at constant  $p_{HCl}$  and  $p_{H_2O}$ ).

The hydrolysis of lower hydrates of chemical mixture ( $CM1/CM2 \cdot nH_2O$ ,  $n = 2, 4, 6$ ) is investigated under fixed  $p_{HCl}$  and fixed  $p_{H_2O}$  as depicted in Figures 12 and 13, respectively. Their

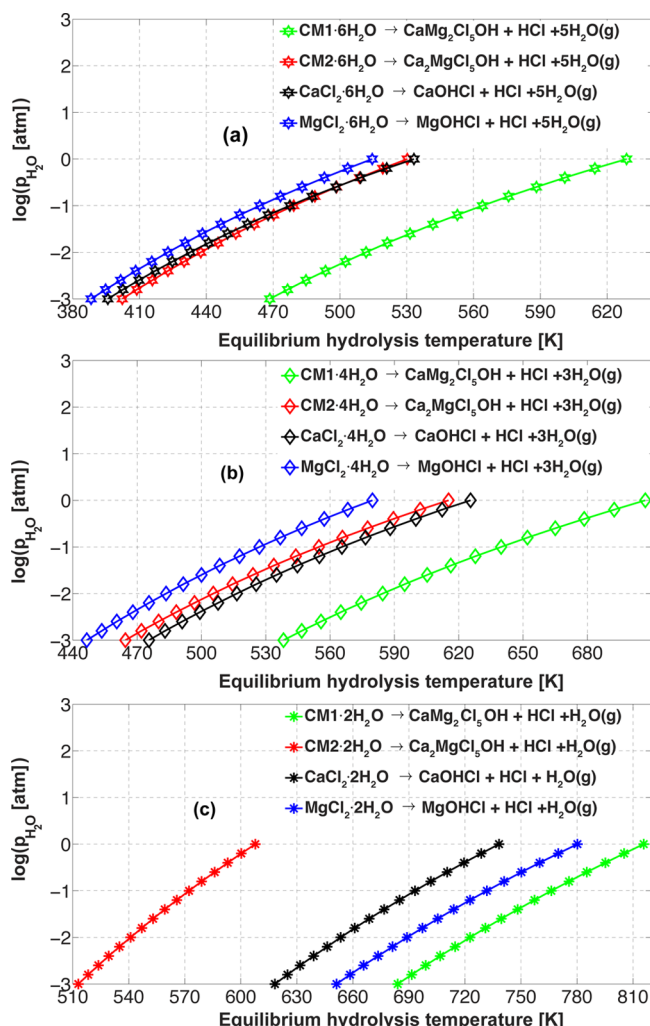


**Figure 12.** Equilibrium product concentrations for the hydrolysis reactions of lower hydrates of CM1 and CM2 at various temperatures and constant partial pressure of hydrate,  $p_o = 1$  atm and  $p_{HCl} = 0.001$ .

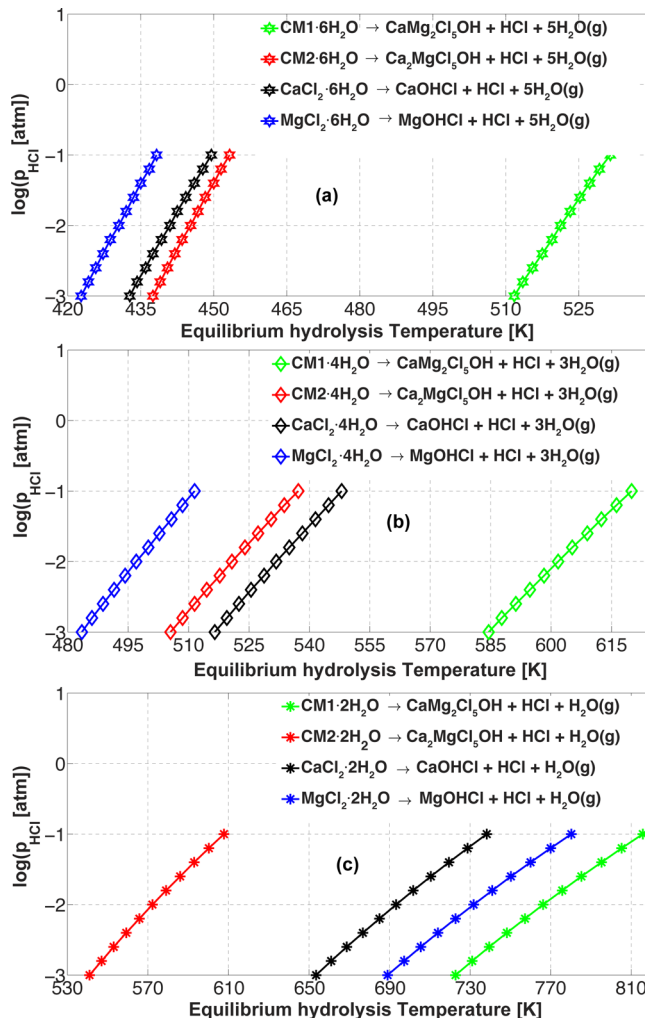


**Figure 13.** Equilibrium product concentrations for the hydrolysis reactions of lower hydrates of CM1 and CM2 at various temperatures and constant partial pressure of hydrate,  $p_o = 1$  atm and  $p_{H_2O} = 0.01$  atm.

hydrolysis curve is compared with the analogous for the elementary salt hydrate of same  $n$ . The hydrolysis temperature to obtain  $p_{H_2O}$  of 0.001 atm at fixed HCl pressure ( $p_{HCl} = 0.001$  atm) is 469, 403, 396, and 423 K for the hexahydrate of CM1, CM2,  $\text{CaCl}_2$ , and  $\text{MgCl}_2$ , respectively (refer to Figure 12). The equivalent temperatures for the tetrahydrate of CM1, CM2,  $\text{CaCl}_2$ , and  $\text{MgCl}_2$  are 538, 464, 475, and 446 K, respectively. For the dihydrate of CM1, CM2,  $\text{CaCl}_2$ , and  $\text{MgCl}_2$ , the corresponding computed temperatures are 684, 513, 618, and 653 K, respectively. The onset temperature of HCl formation pressure of 0.001 atm at fixed  $p_{H_2O}$  of 0.01 atm are 512, 438, 433, and 423 K for the hexahydrate of CM1, CM2,  $\text{CaCl}_2$ , and  $\text{MgCl}_2$ , respectively (refer to Figure 13). The equivalent temperatures for the tetrahydrate of CM1, CM2,  $\text{CaCl}_2$ , and  $\text{MgCl}_2$  are 584, 505, 516, and 483 K, respectively. For the dihydrate of CM1, CM2,  $\text{CaCl}_2$ , and  $\text{MgCl}_2$  the obtained temperatures are of 723, 547, 653, and 689 K, respectively. The onset of hydrolysis temperature clearly indicates that the hydrolysis resistance of the CM1 lower hydrates is greater than that of the CM2 hydrates. The hydrolysis resistance of the chemical mixture is also observed to

be higher when compared with their elementary salt hydrates (except for  $\text{CM2}\cdot 2\text{H}_2\text{O}$ ).

The gradient for all the equilibrium dehydration and hydrolysis curves is presented in Tables S10 and S11 of Supporting Information. The gradient of CM1 higher hydrates is larger than that of CM2 higher hydrates, and therefore CM2 higher hydrates offer a wider range of operational window when compared with CM1 higher hydrates. In lower hydrates (except  $\text{CM2}\cdot 2\text{H}_2\text{O}$ ), the gradient of the chemical mixture is lower than that of the elementary salt hydrates, and thus the chemical mixing increases the window of operation. In hydrolysis, the gradient at fixed  $p_{H_2O}$  is always greater than at fixed  $p_{HCl}$ . Thus, at any fixed  $p_{H_2O}$  a small window of  $p_{HCl}$  could be observed, while at any fixed  $p_{HCl}$  a large window of  $p_{H_2O}$  could be observed. In the operating range of the TCM for solar application, hydrolysis in  $\text{MgCl}_2$  hydrates can be significantly reduced by chemical mixing. By optimizing the chemical mixing ratio, the undesirable side reaction can be reduced, which will improve the durability of the storage cycle. Additionally, chemical mixing also increases the operation window of thermolysis reactions.

## CONCLUSIONS

Chemical mixing is an emerging approach to improve the durability of thermochemical heat storage materials. Our aim is to enhance hydrolysis resistance by chemical mixing of chloride-based salt hydrates. We have carried out GGA-DFT calculations to obtain the optimized structure of various chemical mixture hydrates ( $\text{CaMg}_2\text{Cl}_6$  (CM1)/ $\text{Ca}_2\text{MgCl}_6$  (CM2) $\cdot n\text{H}_2\text{O}$ ;  $n = 0, 2, 4, 6, 8, 10, 12$ ), as well as their Bader atomic charges and vibrational frequencies. The present calculations reveal that the enthalpy change for proton removal, which is an important step in hydrolysis, from  $\text{CaCl}_2\cdot 2\text{H}_2\text{O}$  is 72.5% higher than from  $\text{MgCl}_2\cdot 2\text{H}_2\text{O}$ . Thus,  $\text{CaCl}_2\cdot 2\text{H}_2\text{O}$  has higher hydrolysis resistance than  $\text{MgCl}_2\cdot 2\text{H}_2\text{O}$ , which confirms our previous DFT results.<sup>52</sup> The enthalpies of formation of CM1 and CM2 from their elementary salts are  $-65.5$  and  $-69.1$  kcal/mol. Therefore, CM2 is 3.6 kcal/mol more stable than CM1.

The vibrational frequency analysis reveals that a red-shift in the O–H bonds of the chemical mixtures is observed when comparing with the spectra of an isolated  $\text{H}_2\text{O}$  molecule. The extent of the O–H bond weakening depends on the hydration strength and hydrogen bonding in the chemical mixtures. The Bader topological based bonding indicators reveal that the hydration strength of the outer atoms (Mg in CM1 and Ca in CM2) continuously decreases with increasing  $n$ .

To assess the possibility of higher hydrates formation, we compared the Mg/Ca–Cl bond order in chemical mixtures and elementary salt hydrates. The bond order of Mg–Cl drops from 0.414 to 0.220 in CM1 hydrates, and from 0.622 to 0.005 in  $\text{MgCl}_2$  hydrates as  $n$  varies from 0 to 6. Similarly, the bond order of Ca–Cl drops from 0.368 to 0.220 in CM2 hydrates, and from 0.497 to 0.009 in  $\text{CaCl}_2$  hydrates as  $n$  varies from 0 to 6. As a consequence, CM1 and CM2 can even form higher hydrates ( $n > 6$ ), whereas the elementary salt hydrates of  $\text{CaCl}_2$  and  $\text{MgCl}_2$  can not. The atomic charge distribution reveals that the stability and the hydration strength of the chemical mixture hydrates are dominated by electrostatic interactions.

The hydrolysis enthalpy of CM1 lower hydrates ( $n < 6$ ) is  $\approx 15$  kcal/mol higher than that of CM2 lower hydrates. Comparing chemical mixing with physical mixing, we observe

that the chemical mixing lowers the binding enthalpy with respect to the physical ones.

Structural properties, electronic ground state energies and harmonic frequencies are used to quantify the Gibbs free energy of each reactant and product at a given temperature ( $T$ ) and pressure ( $p$ ). The thermodynamic approach is used to derive the equilibrium product composition of thermolysis at various  $T$  and  $p$  conditions for the chemical mixture hydrates. The calculated effect of temperature on the thermolysis of the investigated chemical mixtures is observed to be similar to the experimental/theoretical thermolysis results for the  $\text{CaCl}_2$  and  $\text{MgCl}_2$  hydrates.<sup>14,60</sup> The dehydration enthalpies of CM1·12H<sub>2</sub>O, CM1·8H<sub>2</sub>O, and CM2·H<sub>2</sub>O are found to be less than 10 kcal/(mol K), and their dehydration starts at subzero temperatures, indicating that they are not stable at room temperature. The higher hydrates of CM2 dehydrate in the temperature range of 297 to 551 K, and CM1 × 10H<sub>2</sub>O in the temperature range of 290 to 408 K. The rise in the dehydration temperature due to chemical mixing at  $p_{\text{H}_2\text{O}} = 1 \text{ atm}$  is from 18 to 128 K and from 136 to 252 K in hexa- and tetrahydrate of CM1 and CM2, respectively, when compared with their elementary salt hydrates of the same  $n$ . In CM1·2H<sub>2</sub>O, the dehydration temperature is increased by 211 K, while in CM2·2H<sub>2</sub>O it is decreased by 191 K. Thus, the chemical composition and hydration number of the chemical mixture can be used to tune the dehydration temperature region.

The competing hydrolysis reactions of CM1/CM2·nH<sub>2</sub>O are investigated under constant  $p_{\text{HCl}}$  and  $p_{\text{H}_2\text{O}}$ . The onset temperature of HCl formation (hydrolysis) is obtained at very low HCl pressure ( $p_{\text{HCl}} = 0.001 \text{ atm}$ ) under different temperature and water vapor pressure conditions. The onset of hydrolysis ( $p_{\text{HCl}} = 0.001 \text{ atm}$  at constant  $p_{\text{H}_2\text{O}} = 0.01 \text{ atm}$ ) in higher hydrates of CM2 is above 419 K, while for CM1 × 10H<sub>2</sub>O is 384 K. The hydrolysis trend for lower hydrates is opposite to higher hydrates. The rise in onset of hydrolysis temperature for hexa-, tetra- and dihydrates of CM1 is 79 K, 68 and 70 K when compared to the  $\text{CaCl}_2$  hydrates of the same  $n$ , under similar conditions. The CM2·6H<sub>2</sub>O increases the onset of hydrolysis temperature by 5 K, when compared with  $\text{CaCl}_2$ ·6H<sub>2</sub>O. The tetra- and dihydrate of CM2 decrease the onset of the hydrolysis temperature by 11 and 106 K, when compared with the tetra- and dihydrate of  $\text{CaCl}_2$ . Thus, the chemical mixing improves the hydrolysis resistance in all the cases, except for CM2·4H<sub>2</sub>O and CM2·2H<sub>2</sub>O.

In higher hydrates, CM2 has a smaller gradient of equilibrium dehydration/hydrolysis curves when compared with CM1 (Figure S10 and Table S10 of Supporting Information). Further, for the lower hydrates of the studied chemical mixtures, the gradients of the equilibrium dehydration/hydrolysis curves are always smaller than that for the elementary salt hydrates with same  $n$ , except CM2·2H<sub>2</sub>O (Figures 11, 12 and 13, and Table S11 of Supporting Information). Therefore, the chemical mixing not only improves the hydrolysis resistance but also increases the window of operation.

Given the lack of experimental studies on the chemical mixtures, it can be concluded from the present study that the chemical mixtures of  $\text{CaCl}_2$  hydrates with  $\text{MgCl}_2$  are potentially good candidates for long-term seasonal heat storage. It is expected that these hydrates can improve the hydrolysis resistance compared to  $\text{MgCl}_2$  hydrates and therefore enhance the durability of the system.

## ASSOCIATED CONTENT

### Supporting Information

The Supporting Information is available free of charge on the ACS Publications website at DOI: [10.1021/acs.jpcc.7b05245](https://doi.org/10.1021/acs.jpcc.7b05245).

Molecular structure of chemical mixtures, tabulated bond lengths and Bader charges, Gibbs free energy calculations, bonding indicators, and equilibrium curve properties (PDF)

## AUTHOR INFORMATION

### Corresponding Author

\*(S.V.N.) E-mail: [S.V.Nedea@tue.nl](mailto:S.V.Nedea@tue.nl).

### ORCID

A. D. Pathak: [0000-0003-4764-9088](https://orcid.org/0000-0003-4764-9088)

### Notes

The authors declare no competing financial interest.

## ACKNOWLEDGMENTS

This work is part of the Industrial Partnership Programme (IPP) "Computational sciences for energy research" of the Foundation for Fundamental Research on Matter (FOM), which is part of The Netherlands Organisation for Scientific Research (NWO). This research programme is cofinanced by Shell Global Solutions International B.V. The DFT calculations have been performed by using HPC resources on the Cartesius supercomputer.

## REFERENCES

- (1) *Renewable Energy Progress Report*; European Commission: Brussels, Belgium, 2015.
- (2) Gil, A.; Medrano, M.; Martorell, I.; Lazaro, A.; Dolado, P.; Zalba, B.; Cabeza, L. F. State of the Art on High Temperature Thermal Energy Storage for Power Generation. Part 1 - Concepts, Materials and Modellization. *Renewable Sustainable Energy Rev.* **2010**, *14*, 31–55.
- (3) Ervin, G. Solar Heat Storage Using Chemical Reactions. *J. Solid State Chem.* **1977**, *22*, 51–61.
- (4) Zondag, H.; Kikkert, B.; Smeding, S.; de Boer, R.; Bakker, M. Prototype Thermochemical Heat Storage with Open Reactor System. *Appl. Energy* **2013**, *109*, 360–365.
- (5) Pinel, P.; Cruickshank, C. A.; Beausoleil-Morrison, I.; Wills, A. A Review of Available Methods for Seasonal Storage of Solar Thermal Energy in Residential Applications. *Renewable Sustainable Energy Rev.* **2011**, *15*, 3341–3359.
- (6) N'Tsoukpo, K. E.; Schmidt, T.; Rammelberg, H. U.; Watts, B. A.; Ruck, W. K. A Systematic Multi-step Screening of Numerous Salt Hydrates for Low Temperature Thermochemical Energy Storage. *Appl. Energy* **2014**, *124*, 1–16.
- (7) Abedin, A. H.; Rosen, M. A. A Critical Review of Thermochemical Energy Storage Systems. *Open Renewable Energy J.* **2011**, *4*, 42.
- (8) Aydin, D.; Casey, S. P.; Riffat, S. The Latest Advancements on Thermochemical Heat Storage Systems. *Renewable Sustainable Energy Rev.* **2015**, *41*, 356–367.
- (9) Cot-Gores, J.; Castell, A.; Cabeza, L. F. Thermochemical Energy Storage and Conversion: A-state-of-the-art review of the Experimental Research under Practical Conditions. *Renewable Sustainable Energy Rev.* **2012**, *16*, 5207–5224.
- (10) Carrillo, A.; Sastre, D.; Serrano, D.; Pizarro, P.; Coronado, J. Revisiting the BaO<sub>2</sub>/BaO Redox Cycle for Solar Thermochemical Energy Storage. *Phys. Chem. Chem. Phys.* **2016**, *18*, 8039–8048.
- (11) Carrillo, A. J.; Serrano, D. P.; Pizarro, P.; Coronado, J. M. Thermochemical Heat Storage Based on the Mn<sub>2</sub>O<sub>3</sub>/Mn<sub>3</sub>O<sub>4</sub> Redox Couple: Influence of the Initial Particle Size on the Morphological Evolution and Cyclability. *J. Mater. Chem. A* **2014**, *2*, 19435–19443.

- (12) Xu, J.; Wang, R.; Li, Y. A Review of Available Technologies for Seasonal Thermal Energy Storage. *Sol. Energy* **2014**, *103*, 610–638.
- (13) Pardo, P.; Deydier, A.; Anxionnaz-Minvielle, Z.; Rougé, S.; Cabassud, M.; Cognet, P. A Review on High Temperature Thermochemical Heat Energy Storage. *Renewable Sustainable Energy Rev.* **2014**, *32*, 591–610.
- (14) Kipouros, G. J.; Sadoway, D. R. A Thermochemical Analysis of the Production of Anhydrous  $MgCl_2$ . *J. Light Met.* **2001**, *1*, 111–117.
- (15) Dolezal, H. Dehydration of Magnesium Chloride. 1976; US Patent US 3,962,408.
- (16) Sivilotti, O. G. Electrolytic Production of Magnesium Metal with Feed Containing Magnesium Chloride Ammoniates. 1995; US Patent US 5,439,563.
- (17) W, K.; S, O.; Y, S.; K, U.; K, Y. Process of Manufacturing Anhydrous Magnesium Chloride. 1974; US Patent US 3,798,314.
- (18) Emons, H.-H.; Voigt, H.; Pohl, T.; Naumann, R. Thermoanalytical Investigations on the Decomposition of Double Salts: Part II. The Decomposition of Double Salts  $MeCl \cdot MgCl_2 \cdot 6H_2O$  ( $Me = NH_4, Rb, Cs$ ). *Thermochim. Acta* **1987**, *121*, 151–163.
- (19) Shoval, S.; Yariv, S.; Kirsh, Y.; Peled, H. The Effect of Alkali Halides on the Thermal Hydrolysis of Magnesium Chloride and Magnesium Bromide. *Thermochim. Acta* **1986**, *109*, 207–226.
- (20) Shkatulov, A.; Aristov, Y. Modification of Magnesium and Calcium Hydroxides with Salts: An Efficient Way to Advanced Materials for Storage of Middle-Temperature Heat. *Energy* **2015**, *85*, 667–676.
- (21) Lane, G. A. *Solar Heat Storage: Latent Heat Materials, Vol II Technology*; CRC Press: Chicago, 1986.
- (22) Mona-Maria Druske, R. H. U.; Neumann, K.; Korhammer, K.; Opel, O.; Ruck, W. *Proceedings of IRES 2016*; 2016.
- (23) Rammelberg, H. U.; Myrau, M.; Schmidt, T.; Ruck, W. *Proceeding of IMPRES 2013, Fukuoka, 04-06*; 2013.
- (24) Posern, K.; Kaps, C. Calorimetric Studies of Thermochemical Heat Storage Materials Based on Mixtures of  $MgSO_4$  and  $MgCl_2$ . *Thermochim. Acta* **2010**, *502*, 73–76.
- (25) Vaccarino, C.; Barbaccia, A.; Frusteri, F.; Galli, G.; Maisano, G. A Low-Temperature Heat Storage System Utilizing Mixtures of Magnesium Salt Hydrates and Ammonium Nitrate. *J. Sol. Energy Eng.* **1985**, *107*, 54–57.
- (26) Lee, W. B.; Egerton, A. C. LXXXIII-Heterogeneous Equilibria between the Chlorides of Calcium, Magnesium, Potassium, and their Aqueous Solutions. Part I. *J. Chem. Soc., Trans.* **1923**, *123*, 706–716.
- (27) Albert, K.; F, P. Method of Treating Brine. 1927; US Patent USUS1627068.
- (28) Prutton, C.; Tower, O. The System Calcium Chloride-Magnesium Chloride-Water1 at 0,-15 and -30°. *J. Am. Chem. Soc.* **1932**, *54*, 3040–3047.
- (29) Clark, J. R.; Evans, H.; Erd, R. Tachyhydrite, Dimagnesium Chloride 12-hydrate. *Acta Crystallogr., Sect. B: Struct. Crystallogr. Cryst. Chem.* **1980**, *36*, 2736–2739.
- (30) Vysotskiy, E. Tachyhydrite in Potash Formations of Cretaceous Age. *Int. Geol. Rev.* **1988**, *30*, 31–35.
- (31) Smeets, B.; Iype, E.; Nedea, S.; Zondag, H.; Rindt, C. A DFT based Equilibrium Study on the Hydrolysis and the Dehydration Reactions of  $MgCl_2$  Hydrates. *J. Chem. Phys.* **2013**, *139*, 124312.
- (32) Iype, E.; Nedea, S. V.; Rindt, C. C.; van Steenhoven, A. A.; Zondag, H. A.; Jansen, A. DFT Study on Characterization of Hydrogen Bonds in the Hydrates of  $MgSO_4$ . *J. Phys. Chem. C* **2012**, *116*, 18584–18590.
- (33) Widdifield, C. M.; Bryce, D. L. A Multinuclear Solid-State Magnetic Resonance and GIPAW DFT Study of Anhydrous Calcium Chloride and its Hydrates. *Can. J. Chem.* **2011**, *89*, 754–763.
- (34) Pathak, A. D.; Nedea, S.; van Duin, A. C.; Zondag, H.; Rindt, C.; Smeulders, D. Reactive Force Field Development for Magnesium Chloride Hydrates and its Application for Seasonal Heat Storage. *Phys. Chem. Chem. Phys.* **2016**, *18*, 15838–15847.
- (35) Weck, P. F.; Kim, E. Solar Energy Storage in Phase Change Materials: First-Principles Thermodynamic Modeling of Magnesium Chloride Hydrates. *J. Phys. Chem. C* **2014**, *118*, 4618–4625.
- (36) Balasubramanian, G.; Ghommeh, M.; Hajj, M. R.; Wong, W. P.; Tomlin, J. A.; Puri, I. K. Modeling of Thermochemical Energy Storage by Salt Hydrates. *Int. J. Heat Mass Transfer* **2010**, *53*, 5700–5706.
- (37) Manz, T.; Limas, N. G. ChargeMol Program for Performing DDEC Analysis, Version 3.4.4, 2016.
- (38) Tang, W.; Sanville, E.; Henkelman, G. A Grid-based Bader Analysis Algorithm without Lattice Bias. *J. Phys.: Condens. Matter* **2009**, *21*, 084204.
- (39) Sanville, E.; Kenny, S. D.; Smith, R.; Henkelman, G. Improved Grid-based Algorithm for Bader Charge Allocation. *J. Comput. Chem.* **2007**, *28*, 899–908.
- (40) Henkelman, G.; Arnaldsson, A.; Jónsson, H. A Fast and Robust Algorithm for Bader Decomposition of Charge Density. *Comput. Mater. Sci.* **2006**, *36*, 354–360.
- (41) Yu, M.; Trinkle, D. R. Accurate and Efficient Algorithm for Bader Charge Integration. *J. Chem. Phys.* **2011**, *134*, 064111.
- (42) Becke, A.; Matta, C. F.; Boyd, R. J. *The Quantum Theory of Atoms in Molecules: from Solid State to DNA and Drug Design*; John Wiley & Sons: 2007.
- (43) Vega, D.; Almeida, D. AIM-UC: An Application for QTAIM Analysis. *J. Comput. Methods Sci. Eng.* **2014**, *14*, 131–136.
- (44) van Santen, R. A. *Modern Heterogeneous Catalysis: An Introduction*; John Wiley & Sons: 2017.
- (45) van Santen, R.; Tranca, I. How molecular is the Chemisorptive Bond? *Phys. Chem. Chem. Phys.* **2016**, *18*, 20868–20894.
- (46) Dronskowski, R.; Bloechl, P. E. Crystal Orbital Hamilton Populations (COHP): Energy-resolved Visualization of Chemical Bonding in Solids Based on Density-Functional Calculations. *J. Phys. Chem.* **1993**, *97*, 8617–8624.
- (47) Deringer, V. L.; Tchougréeff, A. L.; Dronskowski, R. Crystal Orbital Hamilton Population (COHP) Analysis as Projected from Plane-wave Basis Sets. *J. Phys. Chem. A* **2011**, *115*, 5461–5466.
- (48) Maintz, S.; Deringer, V. L.; Tchougréeff, A. L.; Dronskowski, R. Analytic Projection from Plane-wave and PAW Wavefunctions and Application to Chemical-Bonding Analysis in Solids. *J. Comput. Chem.* **2013**, *34*, 2557–2567.
- (49) Perdew, J. P.; Chevary, J.; Vosko, S.; Jackson, K. A.; Pederson, M. R.; Singh, D.; Fiolhais, C. Atoms, Molecules, Solids, and Surfaces: Applications of the Generalized Gradient Approximation for Exchange and Correlation. *Phys. Rev. B: Condens. Matter Mater. Phys.* **1992**, *46*, 6671.
- (50) Te Velde, G. T.; Bickelhaupt, F. M.; Baerends, E. J.; Fonseca Guerra, C.; van Gisbergen, S. J.; Snijders, J. G.; Ziegler, T. Chemistry with ADF. *J. Comput. Chem.* **2001**, *22*, 931–967.
- (51) Perdew, J. P.; Burke, K.; Ernzerhof, M. Generalized Gradient Approximation Made Simple. *Phys. Rev. Lett.* **1996**, *77*, 3865.
- (52) Pathak, A. D.; Nedea, S.; Zondag, H.; Rindt, C.; Smeulders, D. A DFT-based Comparative Equilibrium Study of Thermal Dehydration and Hydrolysis of  $CaCl_2$  Hydrates and  $MgCl_2$  Hydrates for Seasonal Heat Storage. *Phys. Chem. Chem. Phys.* **2016**, *18*, 10059–10069.
- (53) Pathak, A.; Nedea, S. V.; Zondag, H. A.; Rindt, C. C. M.; Smeulders, D. M. A DFT Based Equilibrium Study of a Chemical Mixture Tachyhydrite and their Lower Hydrates for Long Term Heat Storage. *J. Phys.: Conf. Ser.* **2016**, *745*, 032003.
- (54) Oganov, A. R.; Glass, C. W. Crystal structure prediction using ab initio Evolutionary Techniques: Principles and Applications. *J. Chem. Phys.* **2006**, *124*, 244704.
- (55) Landrum, G. A.; Dronskowski, R. The Orbital Origins of Magnetism: from Atoms to Molecules to Ferromagnetic Alloys. *Angew. Chem., Int. Ed.* **2000**, *39*, 1560–1585.
- (56) Hoffmann, R. Interaction of Orbitals through Space and through Bonds. *Acc. Chem. Res.* **1971**, *4*, 1–9.
- (57) Gonzalez, L.; Mo, O.; Yanez, M. High-level ab-initio versus DFT Calculations on  $(H_2O_2)_2$  and  $H_2O_2 \cdot H_2O$  Complexes as Prototypes of Multiple Hydrogen Bond Systems. *J. Comput. Chem.* **1997**, *18*, 1124–1135.
- (58) Engdahl, A.; Nelander, B. Water in Krypton Matrices. *J. Mol. Struct.* **1989**, *193*, 101–109.

(59) Wang, W.; Chen, S. Theoretical Study on the Thermolysis Mechanism of Monohydrate Magnesium Chloride. *J. Comput. Sci. Eng.* **2011**, *2*, 79–84.

(60) Zondag, H.; van Essen, M.; Bleijendaal, L.; Cot, J.; Schuitema, R.; van Helden, W.; Planje, W.; Epema, T.; Oversloot, H. Comparison of Reactor Concepts for Thermochemical Storage of Solar Heat. *Proceeding of IRES* 2008.